Density Model for Dwarf and Pygmy Sperm Whales (*Kogia spp.*) for the U.S. East Coast: Supplementary Report

Model Version 5.1

Duke University Marine Geospatial Ecology Laboratory*

2023-05-27

Citation

When citing our methodology or results generally, please cite Roberts et al. (2016, 2023). The complete references appear at the end of this document. We are preparing a new article for a peer-reviewed journal that will eventually replace those. Until that is published, those are the best general citations.

When citing this model specifically, please use this reference:

Roberts JJ, Yack TM, Cañadas A, Fujioka E, Halpin PN, Barco SG, Boisseau O, Chavez-Rosales S, Cole TVN, Cotter MP, Cummings EW, Davis GE, DiGiovanni Jr. RA, Garrison LP, Gowan TA, Jackson KA, Kenney RD, Khan CB, Lockhart GG, Lomac-MacNair KS, McAlarney RJ, McLellan WA, Mullin KD, Nowacek DP, O'Brien O, Pabst DA, Palka DL, Quintana-Rizzo E, Redfern JV, Rickard ME, White M, Whitt AD, Zoidis AM (2022) Density Model for Dwarf and Pygmy Sperm Whales (*Kogia spp.*) for the U.S. East Coast, Version 5.1, 2023-05-27, and Supplementary Report. Marine Geospatial Ecology Laboratory, Duke University, Durham, North Carolina.

Copyright and License

Model Version History

Version	Date	Description
1	2014-10-15	Initial version.
2	2014-11-23	Reconfigured detection hierarchy and adjusted NARWSS detection functions based on additional information from Tim Cole. Updated documentation.
3	2015-03-06	Added a missing sighting from the Gulf of Mexico that affected the Oregon II detection function for both study areas. Refitted that detection function and the density model.
3.1	2015-05-14	Updated calculation of CVs. Switched density rasters to logarithmic breaks. No changes to the model.
3.2	2015-10-07	Updated the documentation. No changes to the model. Model files released as supplementary information to Roberts et al. (2016).

*For questions or to offer feedback please contact Jason Roberts (jason.roberts@duke.edu) and Tina Yack (tina.yack@duke.edu)

(continued)

Version	Date	Description
4	2018-04-14	Began update to Roberts et al. (2015) model. Introduced new surveys from AMAPPS, NARWSS, UNCW, VAMSC, and the SEUS NARW teams. Updated modeling methodology. Refitted detection functions and spatial models from scratch using new and reprocessed covariates. Model released as part of a scheduled update to the U.S. Navy Marine Species Density Database (NMSDD).
5	2022-06-20	This model is a major update over the prior version, with substantial additional data, improved statistical methods, and an increased spatial resolution. It was released as part of the final delivery of the U.S. Navy Marine Species Density Database (NMSDD) for the Atlantic Fleet Testing and Training (AFTT) Phase IV Environmental Impact Statement. Several new collaborators joined and contributed survey data: New York State Department of Environmental Conservation, TetraTech, HDR, and Marine Conservation Research. We incorporated additional surveys from all continuing and new collaborators through the end of 2020. (Because some environmental covariates were only available through 2019, certain models only extend through 2019.) We increased the spatial resolution to 5 km and, at NOAA's request, we extended the model further inshore from New York through Maine. We reformulated and refitted all detection functions and spatial models. We updated all enviromental covariates to newer products, when available, and added several covariates to the set of candidates. For models that incorporated dynamic covariates, we estimated model uncertainty using a new method that accounts for both model parameter error and temporal variability.
5.1	2023-05-27	Completed the supplementary report documenting the details of this model. The model itself was not changed.

1 Survey Data

We built this model from data collected between 1998-2019 (Table 1, Figure 1). In keeping with our primary strategy for the 2022 modeling cycle, we excluded data prior to 1998 in order to utilize biological covariates derived from satellite ocean color observations, which were only available for a few months before 1998. We also excluded data after 2019 in order to utilize zooplankton and micronekton biomass estimates from SEAPODYM (Lehodey et al. 2008), which preliminary modeling indicated were were effective spatial covariates but were only available through 2019. We also excluded NEFSC shipboard surveys prior to the start of the AMAPPS program in 2010, as observers on the NEFSC pre-AMAPPS shipboard surveys experienced substantial difficulty distinguishing Kogia from other similarly-sized whales. During AMAPPS, NEFSC undertook a special effort to fully identify all Kogia using new techniques (D. Palka, pers. comm.), resulting in an increased number of Kogia identifications. In order to avoid a temporal bias in density relating to this species identification problem, we excluded NEFSC's pre-AMAPPS shipboard surveys. Finally, we restricted the model to survey transects with sea states of Beaufort 5 or less (for a few surveys we used Beaufort 4 or less) for both aerial and shipboard surveys. We also excluded transects with poor weather or visibility for surveys that reported those conditions.

Table 1: Survey effort and observations considered for this model. Effort is tallied as the cumulative length of on-effort transects. Observations are the number of groups and individuals encountered while on effort. Off effort observations and those lacking an estimate of group size or distance to the group were excluded.

			Effort	Observations		
Institution	Program	Period	1000s km	Groups	Individuals	Mean Group Size
Aerial Surveys						
HDR	Navy Norfolk Canyon	2018-2019	11	9	14	1.6
NEAq	CNM	2017-2019	2	0	0	
NEAq	MMS-WEA	2017-2019	31	0	0	
NEAq	NLPSC	2011-2015	43	0	0	
NEFSC	AMAPPS	2010-2019	89	0	0	
NEFSC	NARWSS	2003-2019	431	0	0	
NEFSC	Pre-AMAPPS	1999-2008	46	1	1	1.0
NYS-DEC/TT	NYBWM	2017-2019	58	0	0	
SEFSC	AMAPPS	2010-2019	111	1	1	1.0
SEFSC	MATS	2002-2005	27	0	0	
UNCW	MidA Bottlenose	2002-2002	17	0	0	
UNCW	Navy Cape Hatteras	2011-2017	34	4	14	3.5
UNCW	Navy Jacksonville	2009-2017	92	2	3	1.5
UNCW	Navy Norfolk Canyon	2015-2017	14	0	0	
UNCW	Navy Onslow Bay	2007-2011	49	0	0	
UNCW	SEUS NARW EWS	2005-2008	114	0	0	
VAMSC	MD DNR WEA	2013-2015	16	0	0	
VAMSC	Navy VACAPES	2016-2017	19	0	0	
VAMSC	VA CZM WEA	2012-2015	21	0	0	
		Total	**1,227**	**17**	**33**	**1.9**
Shipboard Surveys						
NEFSC	AMAPPS	2011-2016	14	74	107	1.4
SEFSC	AMAPPS	2011-2016	14	47	97	2.1
SEFSC	Pre-AMAPPS	1998-2006	27	14	27	1.9
		Total	**55**	**135**	**231**	**1.7**
		Grand Total	**1,283**	**152**	**264**	**1.7**

Table 2: Institutions that contributed surveys used in this model.

Institution	Full Name
HDR	HDR, Inc.
NEAq	New England Aquarium
NEFSC	NOAA Northeast Fisheries Science Center

Table 2: Institutions that contributed surveys used in this model. *(continued)*

Institution	Full Name
NYS-DEC/TT	New York State Department of Environmental Conservation and Tetra Tech, Inc.
SEFSC	NOAA Southeast Fisheries Science Center
UNCW	University of North Carolina Wilmington
VAMSC	Virginia Aquarium & Marine Science Center

Table 3: Descriptions and references for survey programs used in this model.

Program	Description	References
AMAPPS	Atlantic Marine Assessment Program for Protected Species	Palka et al. (2017), Palka et al. (2021)
CNM	Northeast Canyons Marine National Monument Aerial Surveys	Redfern et al. (2021)
MATS	Mid-Atlantic Tursiops Surveys	
MD DNR WEA	Aerial Surveys of the Maryland Wind Energy Area	Barco et al. (2015)
MidA Bottlenose	Mid-Atlantic Onshore/Offshore Bottlenose Dolphin Surveys	Torres et al. (2005)
MMS-WEA	Marine Mammal Surveys of the MA and RI Wind Energy Areas	Quintana-Rizzo et al. (2021), O'Brien et al. (2022)
NARWSS	North Atlantic Right Whale Sighting Surveys	Cole et al. (2007)
Navy Cape Hatteras	Aerial Surveys of the Navy's Cape Hatteras Study Area	McLellan et al. (2018)
Navy Jacksonville	Aerial Surveys of the Navy's Jacksonville Study Area	Foley et al. (2019)
Navy Norfolk Canyon	Aerial Surveys of the Navy's Norfolk Canyon Study Area	Cotter (2019), McAlarney et al. (2018)
Navy Onslow Bay	Aerial Surveys of the Navy's Onslow Bay Study Area	Read et al. (2014)
Navy VACAPES	Aerial Survey Baseline Monitoring in the Continental Shelf Region of the VACAPES OPAREA	Mallette et al. (2017)
NLPSC	Northeast Large Pelagic Survey Collaborative Aerial Surveys	Leiter et al. (2017), Stone et al. (2017)
NYBWM	New York Bight Whale Monitoring Surveys	Zoidis et al. (2021)
Pre-AMAPPS	Pre-AMAPPS Marine Mammal Abundance Surveys	Mullin and Fulling (2003), Garrison et al. (2010), Palka (2006)
SEUS NARW EWS	Southeast U.S. Right Whale Early Warning System Surveys	
VA CZM WEA	Virginia CZM Wind Energy Area Surveys	Mallette et al. (2014), Mallette et al. (2015)

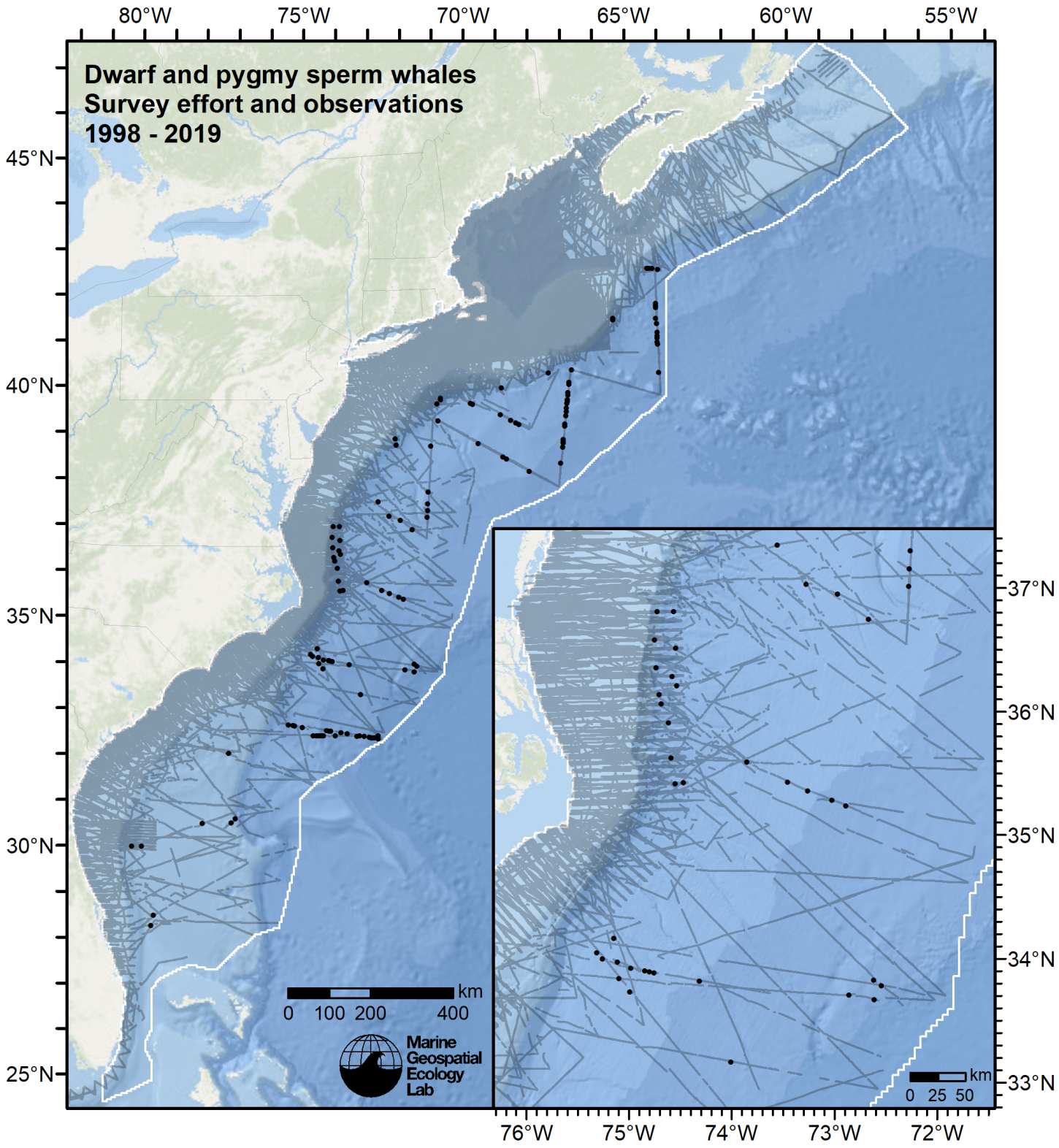

Figure 1: Survey effort and dwarf and pygmy sperm whales observations available for density modeling, after detection functions were applied, and excluded segments and truncated observations were removed.

2 Detection Functions

2.1 With a Taxonomic Covariate

We fitted the detection functions in this section to pools of species with similar detectability characteristics and used the taxonomic identification as a covariate (ScientificName) to account for differences between them. We consulted the literature and observer teams to determine appropriate poolings. We usually employed this approach to boost the counts of observations in the detection functions, which increased the chance that other covariates such as Beaufort sea state could be used to account for differences in observing conditions. When defining the taxonomic covariate, we sometimes had too few observations of species to allocate each of them their own level of the covariate and had to group them together, again consulting the literature and observers for advice on species similarity. Also, when species were observed frequently enough to be allocated their own levels but statistical tests indicated no significant difference between the levels, we usually grouped them together into a single level.

2.1.1 Aerial Surveys

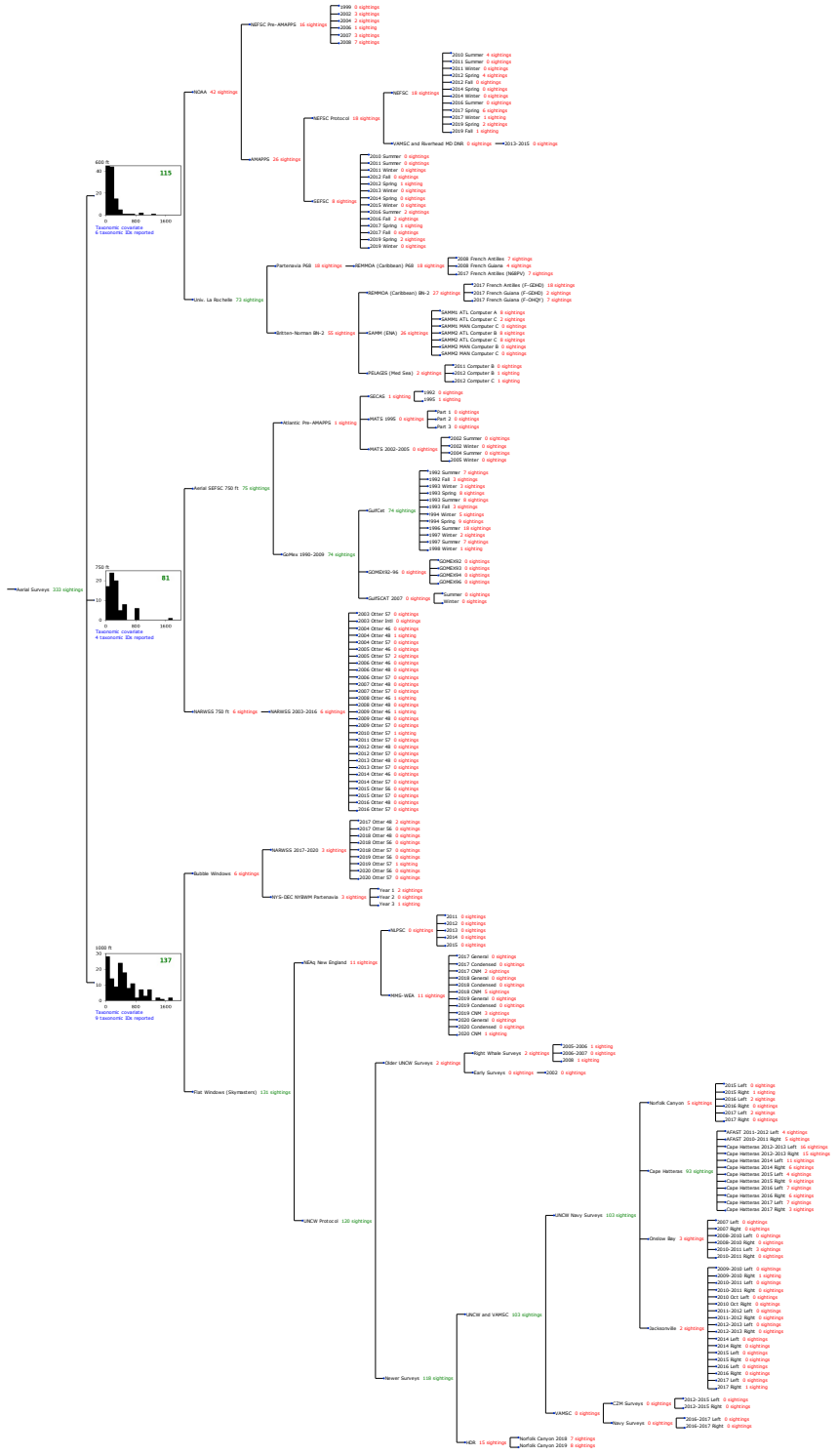

Figure 2: Detection hierarchy for aerial surveys, showing how they were pooled during detectability modeling, for detection functions that pooled multiple taxa and used used a taxonomic covariate to account for differences between them. Each histogram represents a detection function and summarizes the perpendicular distances of observations that were pooled to fit it, prior to truncation. Observation counts, also prior to truncation, are shown in green when they met the recommendation of Buckland et al. (2001) that detection functions utilize at least 60 sightings, and red otherwise. For rare taxa, it was not always possible to meet this recommendation, yielding higher statistical uncertainty. During the spatial modeling stage of the analysis, effective strip widths were computed for each survey using the closest detection function above it in the hierarchy (i.e. moving from right to left in the figure). Surveys that do not have a detection function above them in this figure were either addressed by a detection function presented in a different section of this report, or were omitted from the analysis.

2.1.1.1 600 ft

After right-truncating observations greater than 400 m, we fitted the detection function to the 109 observations that remained (Table 4). The selected detection function (Figure 3) used a hazard rate key function with OriginalScientificName (Figure 4) as a covariate.

Table 4: Observations used to fit the 600 ft detection function.

ScientificName	n
Hyperoodon ampullatus	3
Kogia	23
Mesoplodon	14
Mesoplodon bidens	1
Ziphiidae	33
Ziphius cavirostris	35
Total	**109**

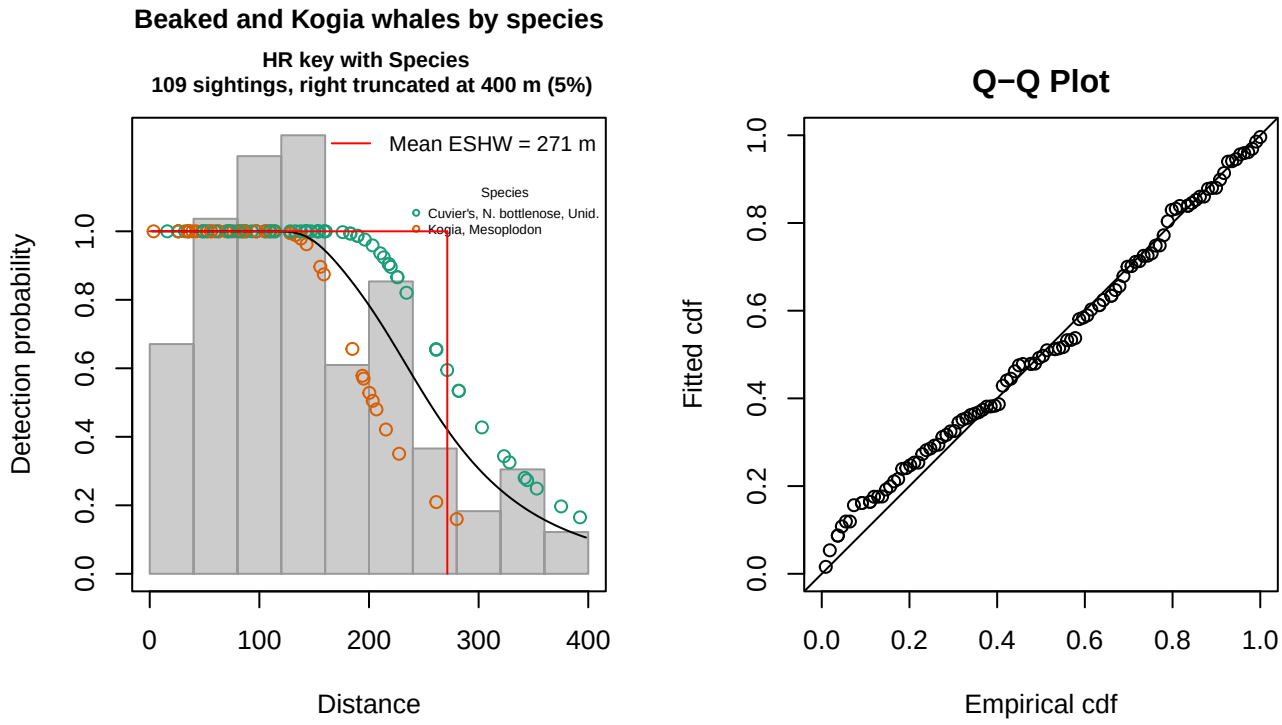

Figure 3: 600 ft detection function and Q-Q plot showing its goodness of fit.

Statistical output for this detection function:

```
Summary for ds object
Number of observations :  109
Distance range         :  0  -  400
AIC                    :  1272.901

Detection function:
 Hazard-rate key function

Detection function parameters
Scale coefficient(s):
                                  estimate        se
(Intercept)                     5.5800164 0.1212472
```

```
OriginalScientificNameKogia, Mesoplodon -0.3454612 0.1492241

Shape coefficient(s):
            estimate        se
(Intercept) 1.474338 0.3977595

                        Estimate          SE         CV
Average p             0.6645919  0.04555694 0.06854874
N in covered region 164.0104361 14.58154672 0.08890621

Distance sampling Cramer-von Mises test (unweighted)
Test statistic = 0.116256  p = 0.510907
```

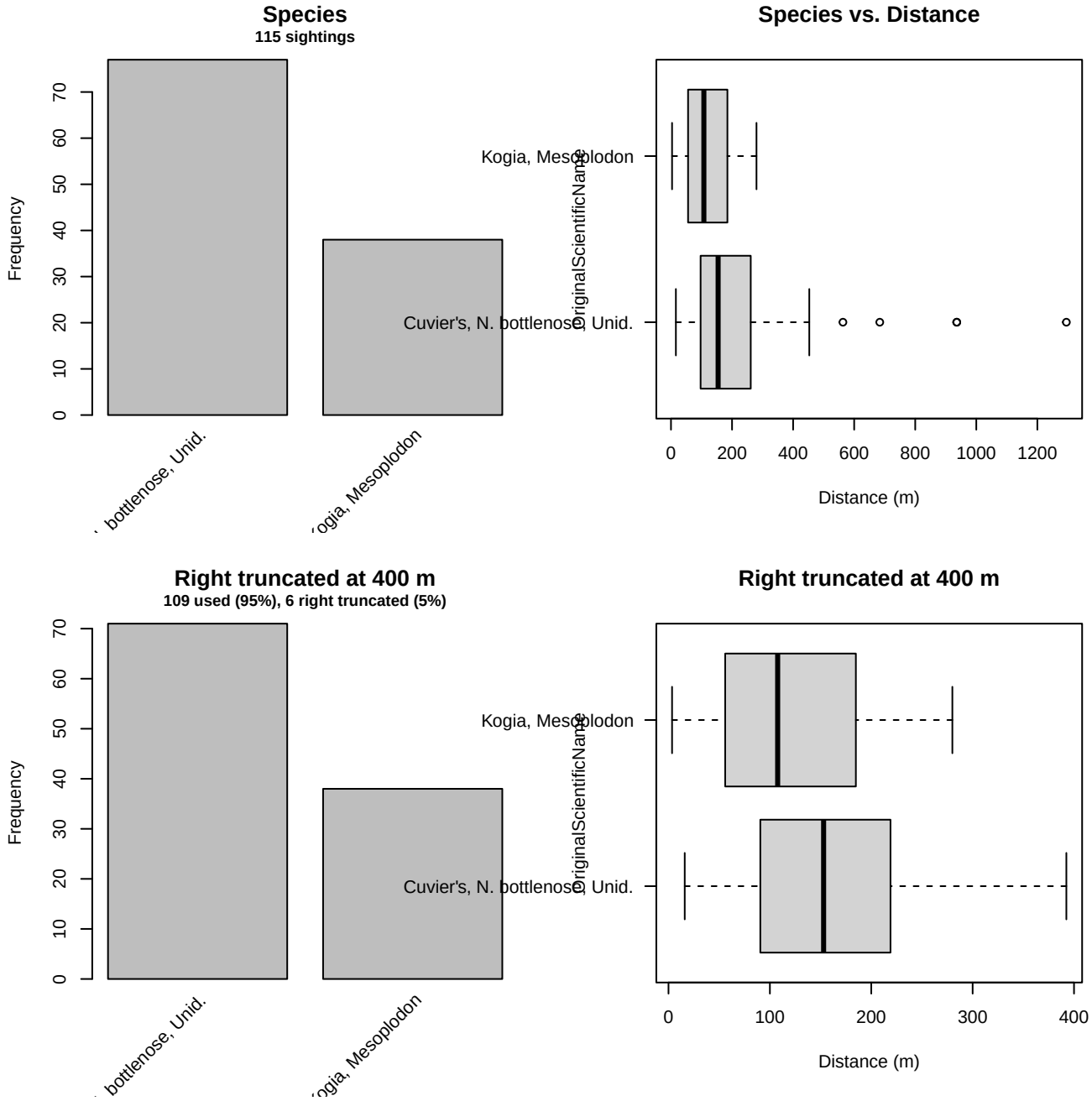

Figure 4: Distribution of the OriginalScientificName covariate before (top row) and after (bottom row) observations were truncated to fit the 600 ft detection function.

2.1.1.2 750 ft

After right-truncating observations greater than 1297 m, we fitted the detection function to the 80 observations that remained (Table 5). The selected detection function (Figure 5) used a hazard rate key function with Beaufort (Figure 6) and OriginalScientificName (Figure 7) as covariates.

Table 5: Observations used to fit the 750 ft detection function.

ScientificName	n
Kogia	55
Mesoplodon	9
Ziphiidae	12
Ziphius cavirostris	4
Total	**80**

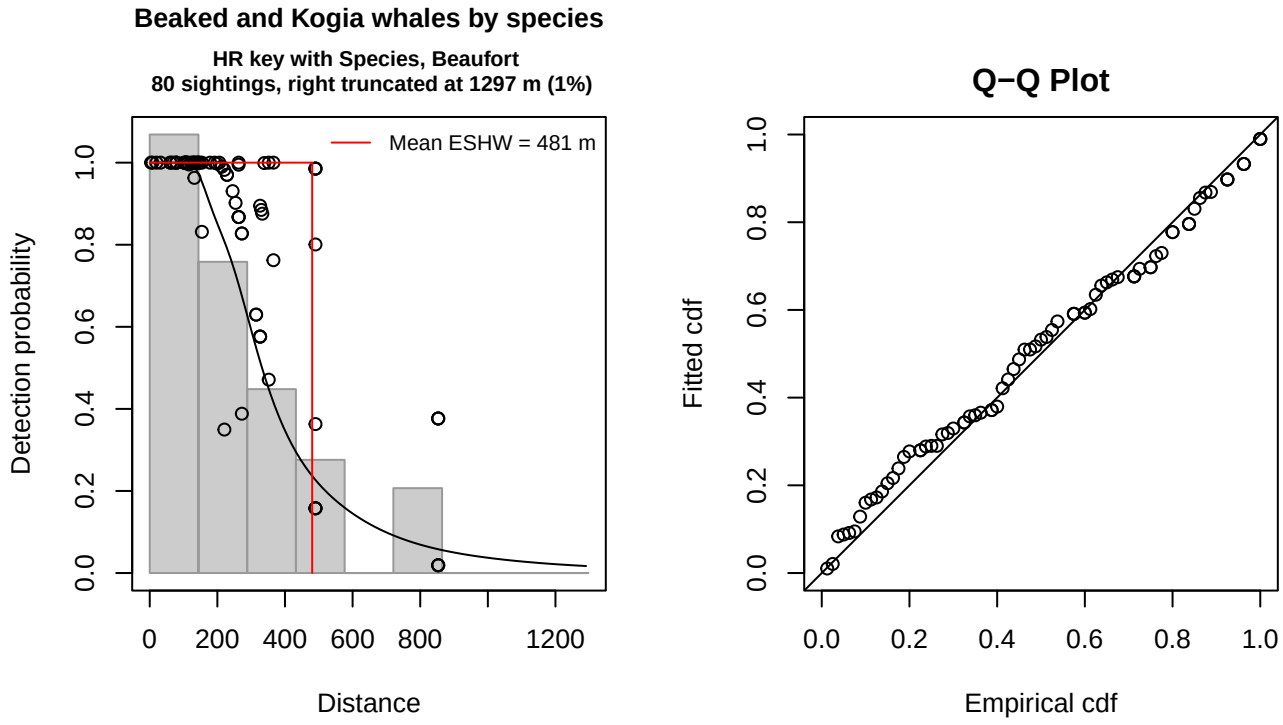

Figure 5: 750 ft detection function and Q-Q plot showing its goodness of fit.

Statistical output for this detection function:

```
Summary for ds object
Number of observations :  80
Distance range         :  0  -  1297
AIC                    :  1037.791

Detection function:
 Hazard-rate key function

Detection function parameters
Scale coefficient(s):
                             estimate        se
(Intercept)                 7.1253756 0.3142159
OriginalScientificNameKogia -0.8097794 0.2203485
Beaufort                    -0.5658239 0.1695498
```

```
Shape coefficient(s):
            estimate        se
(Intercept) 1.375855 0.1977036

                        Estimate          SE        CV
Average p              0.3064062  0.03275229 0.1068917
N in covered region 261.0913218 37.74245080 0.1445565

Distance sampling Cramer-von Mises test (unweighted)
Test statistic = 0.106921  p = 0.551997
```

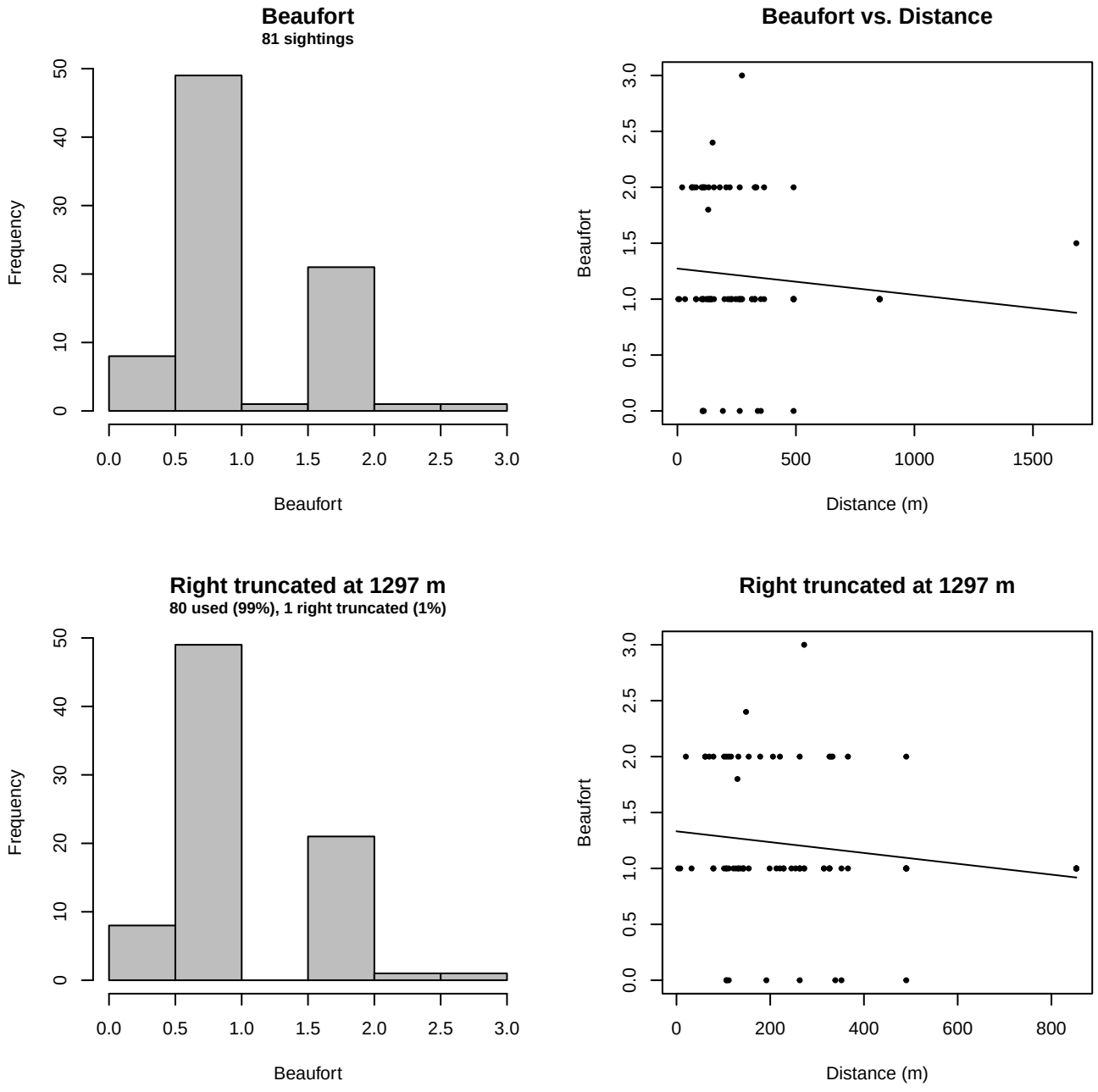

Figure 6: Distribution of the Beaufort covariate before (top row) and after (bottom row) observations were truncated to fit the 750 ft detection function.

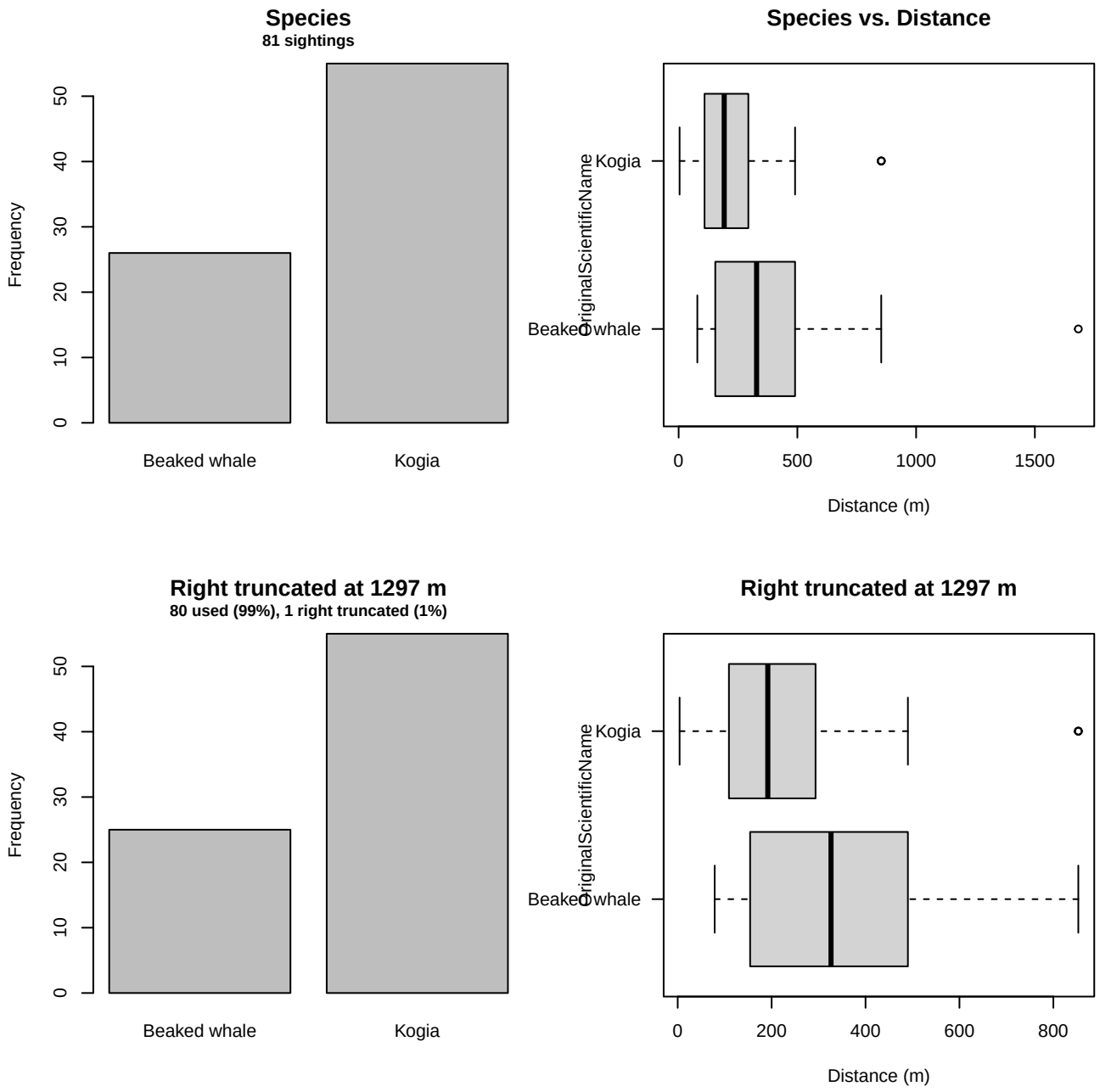

Figure 7: Distribution of the OriginalScientificName covariate before (top row) and after (bottom row) observations were truncated to fit the 750 ft detection function.

2.1.1.3 1000 ft

After right-truncating observations greater than 1250 m, we fitted the detection function to the 131 observations that remained (Table 6). The selected detection function (Figure 8) used a half normal key function with OriginalScientificName (Figure 9) as a covariate.

Table 6: Observations used to fit the 1000 ft detection function.

ScientificName	n
Hyperoodon ampullatus	1
Kogia	14
Kogia sima	1
Mesoplodon	26
Mesoplodon bidens	6
Mesoplodon europaeus	7
Mesoplodon mirus	3
Ziphiidae	11
Ziphius cavirostris	62
Total	**131**

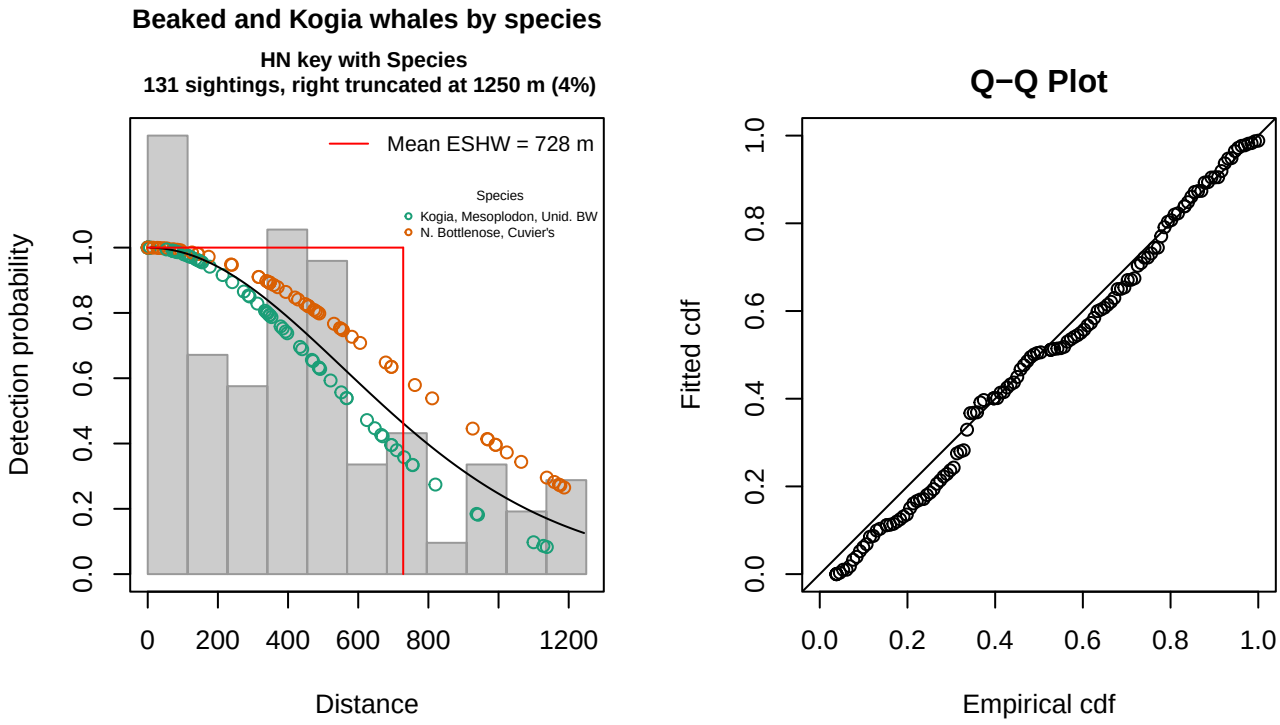

Figure 8: 1000 ft detection function and Q-Q plot showing its goodness of fit.

Statistical output for this detection function:

```
Summary for ds object
Number of observations :  131
Distance range         :  0  -  1250
AIC                    :  1830.819

Detection function:
 Half-normal key function

Detection function parameters
Scale coefficient(s):
                                          estimate        se
(Intercept)                              6.2340705 0.1031336
OriginalScientificNameN. Bottlenose, Cuvier's 0.3570255 0.1899459

                     Estimate          SE         CV
```

```
Average p             0.5712474  0.04000868 0.07003740
N in covered region 229.3227075 20.84792919 0.09091088

Distance sampling Cramer-von Mises test (unweighted)
Test statistic = 0.133457  p = 0.444164
```

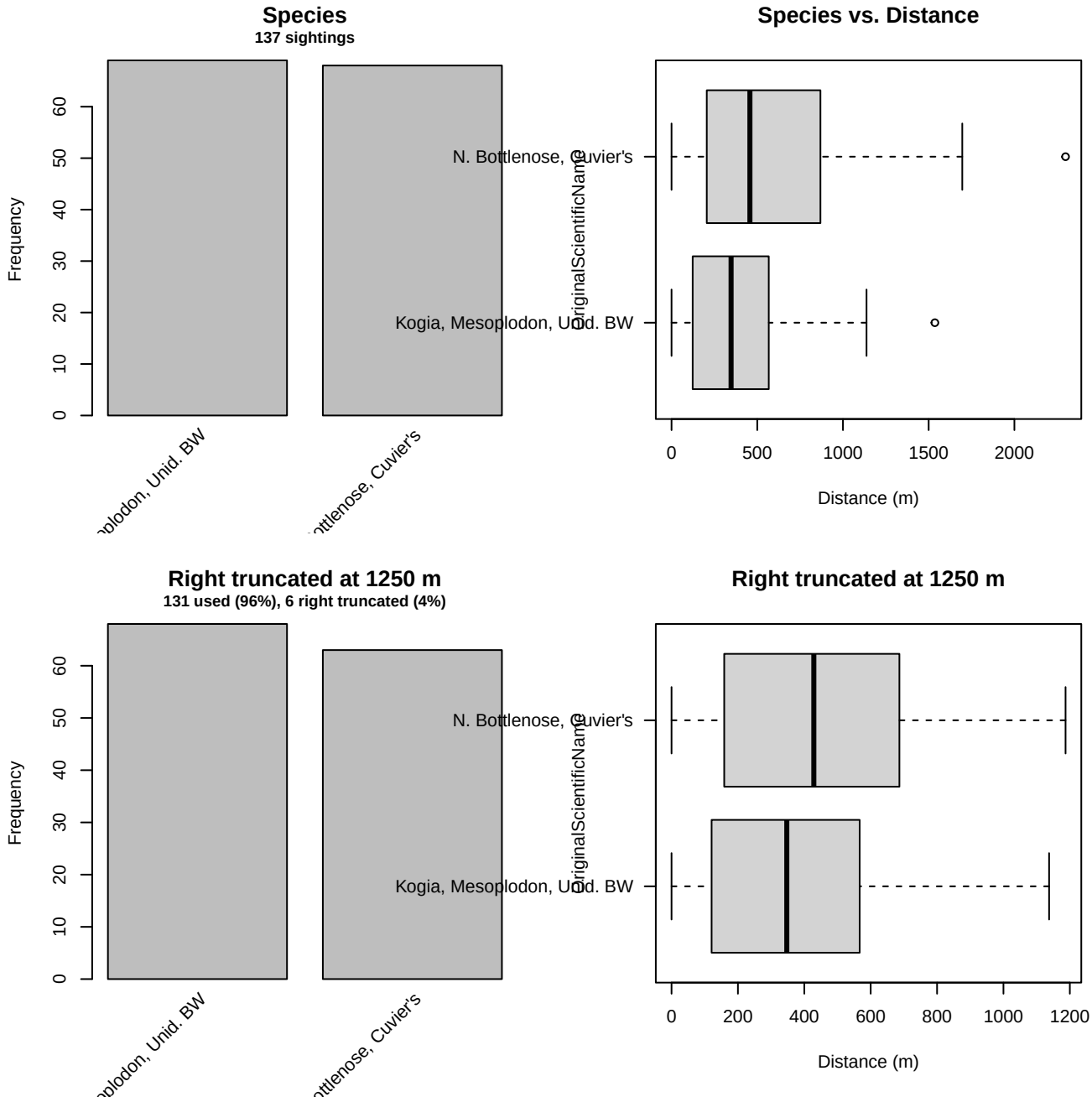

Figure 9: Distribution of the OriginalScientificName covariate before (top row) and after (bottom row) observations were truncated to fit the 1000 ft detection function.

2.1.2 Shipboard Surveys

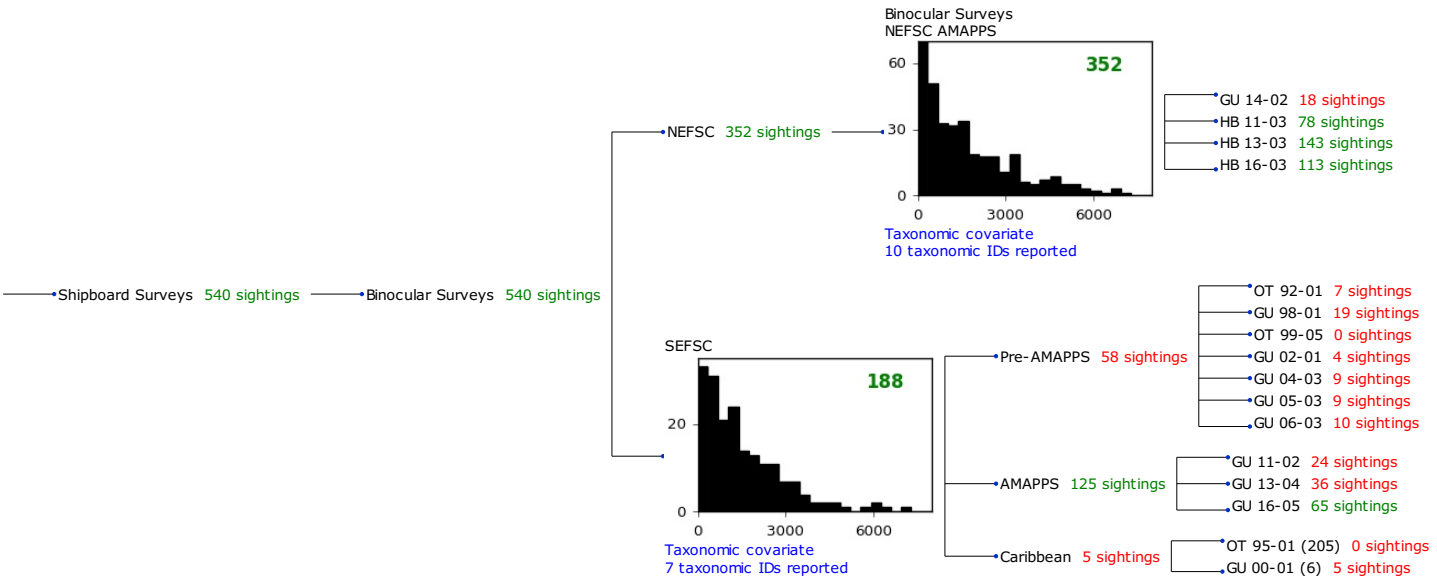

Figure 10: Detection hierarchy for shipboard surveys, showing how they were pooled during detectability modeling, for detection functions that pooled multiple taxa and used used a taxonomic covariate to account for differences between them. Each histogram represents a detection function and summarizes the perpendicular distances of observations that were pooled to fit it, prior to truncation. Observation counts, also prior to truncation, are shown in green when they met the recommendation of Buckland et al. (2001) that detection functions utilize at least 60 sightings, and red otherwise. For rare taxa, it was not always possible to meet this recommendation, yielding higher statistical uncertainty. During the spatial modeling stage of the analysis, effective strip widths were computed for each survey using the closest detection function above it in the hierarchy (i.e. moving from right to left in the figure). Surveys that do not have a detection function above them in this figure were either addressed by a detection function presented in a different section of this report, or were omitted from the analysis.

2.1.2.1 NEFSC AMAPPS

After right-truncating observations greater than 6000 m, we fitted the detection function to the 346 observations that remained (Table 7). The selected detection function (Figure 11) used a hazard rate key function with Beaufort (Figure 12) and OriginalScientificName (Figure 13) as covariates.

Table 7: Observations used to fit the NEFSC AMAPPS detection function.

ScientificName	n
Kogia	22
Kogia breviceps	26
Kogia sima	26
Mesoplodon	69
Mesoplodon bidens	25
Mesoplodon densirostris	1
Mesoplodon europaeus	9
Mesoplodon mirus	5
Ziphiidae	66
Ziphius cavirostris	97
Total	**346**

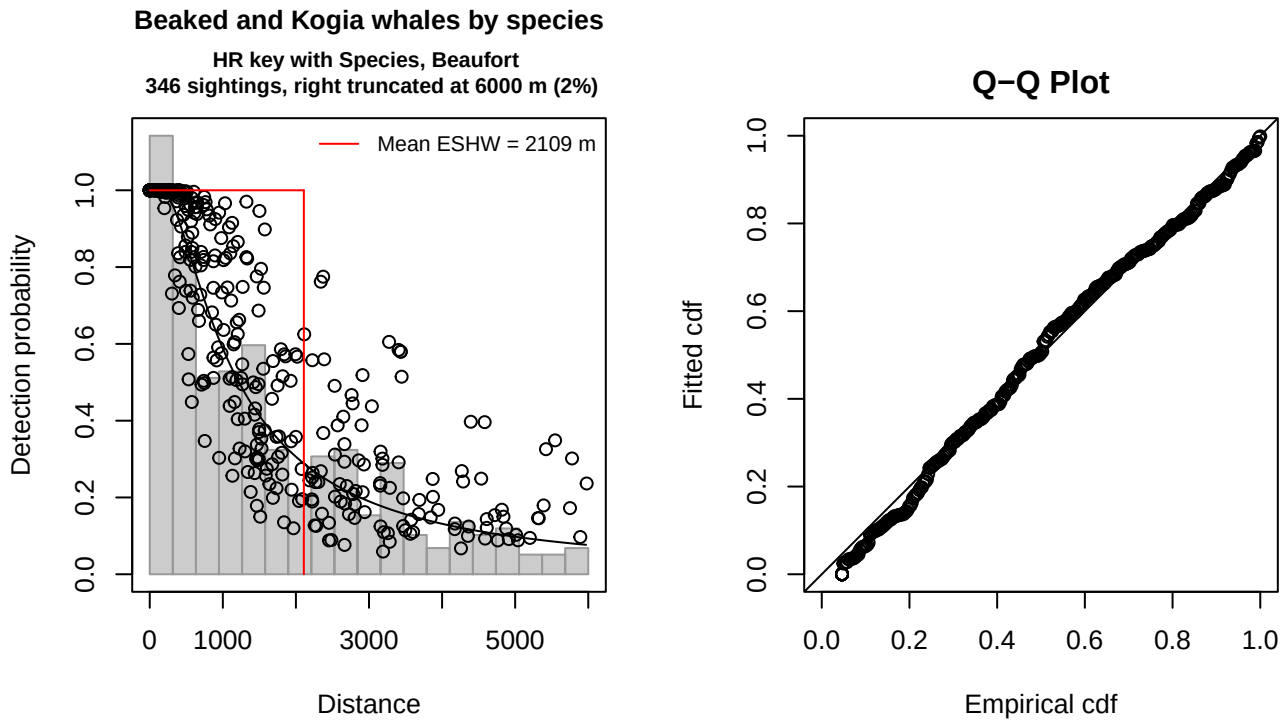

Figure 11: NEFSC AMAPPS detection function and Q-Q plot showing its goodness of fit.

Statistical output for this detection function:

```
Summary for ds object
Number of observations :  346
Distance range         :  0  -  6000
AIC                    :  5785.351

Detection function:
 Hazard-rate key function

Detection function parameters
Scale coefficient(s):
                                        estimate        se
(Intercept)                            7.3858955 0.2987960
OriginalScientificNameMesoplodon spp.  0.4227606 0.2980810
OriginalScientificNameUnid. beaked whale  1.0597067 0.3490831
OriginalScientificNameZiphius cavirostris  0.5834157 0.3145854
Beaufort                              -0.4013373 0.1086192

Shape coefficient(s):
             estimate        se
(Intercept) 0.3840272 0.1226579

                      Estimate           SE         CV
Average p             0.310415   0.02991647 0.09637573
N in covered region 1114.636870 119.01013562 0.10677032

Distance sampling Cramer-von Mises test (unweighted)
Test statistic = 0.147958  p = 0.395858
```

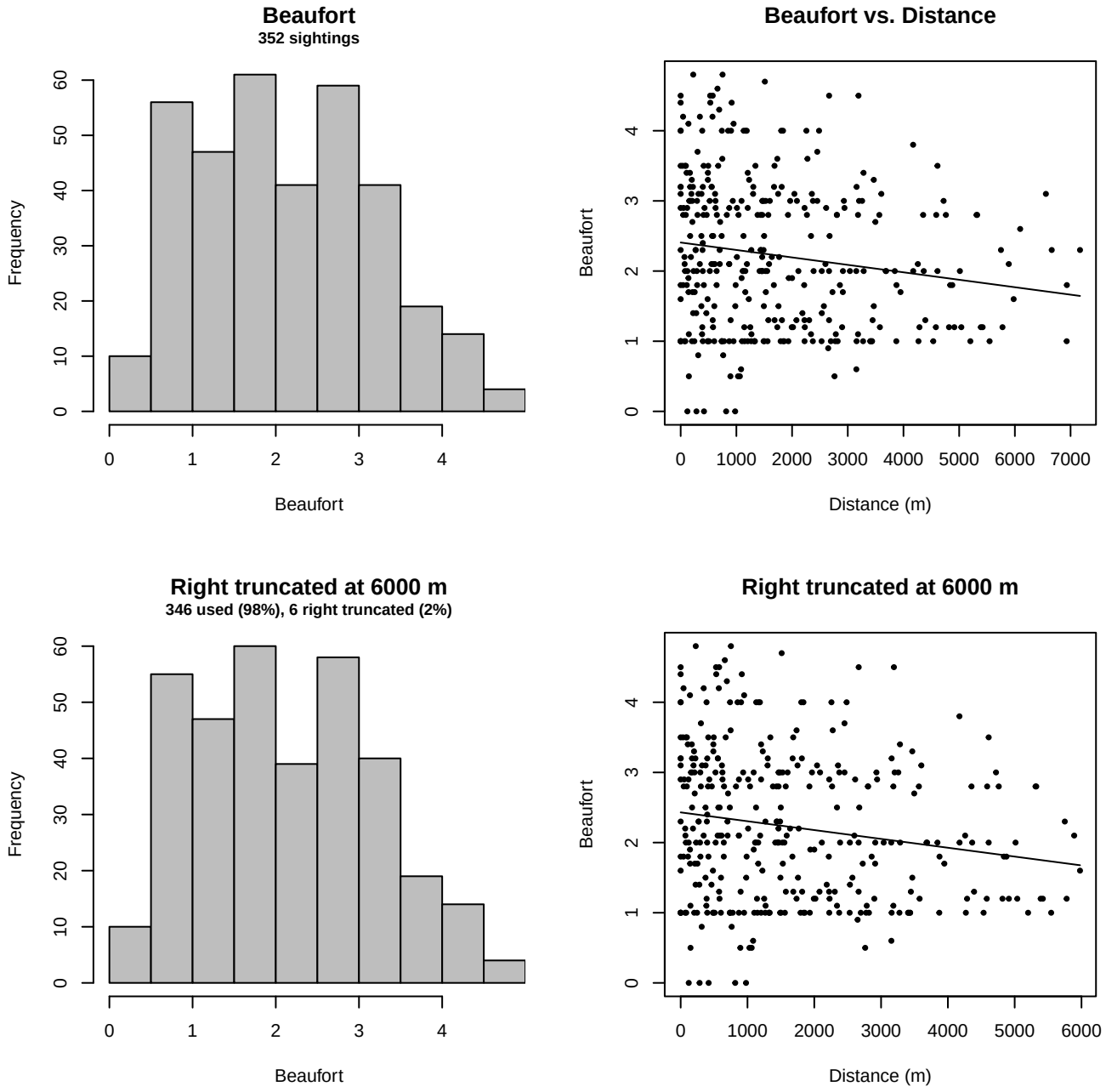

Figure 12: Distribution of the Beaufort covariate before (top row) and after (bottom row) observations were truncated to fit the NEFSC AMAPPS detection function.

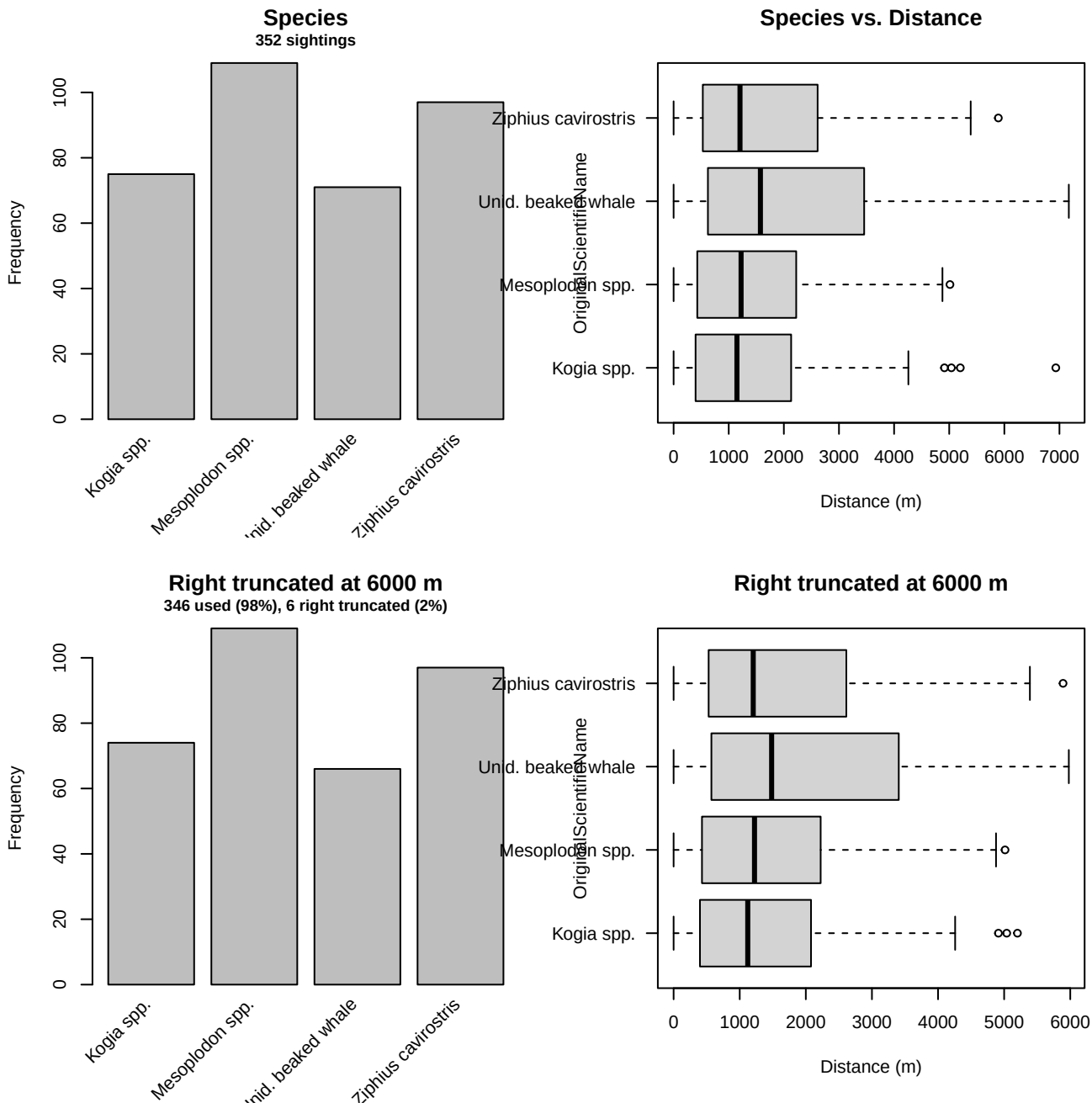

Figure 13: Distribution of the OriginalScientificName covariate before (top row) and after (bottom row) observations were truncated to fit the NEFSC AMAPPS detection function.

2.1.2.2 SEFSC

After right-truncating observations greater than 5000 m, we fitted the detection function to the 182 observations that remained (Table 8). The selected detection function (Figure 14) used a half normal key function with Beaufort (Figure 15) and OriginalScientificName (Figure 16) as covariates.

Table 8: Observations used to fit the SEFSC detection function.

ScientificName	n
Kogia	60
Kogia sima	9
Mesoplodon	37
Mesoplodon densirostris	3
Mesoplodon europaeus	1
Ziphiidae	52
Ziphius cavirostris	20
Total	**182**

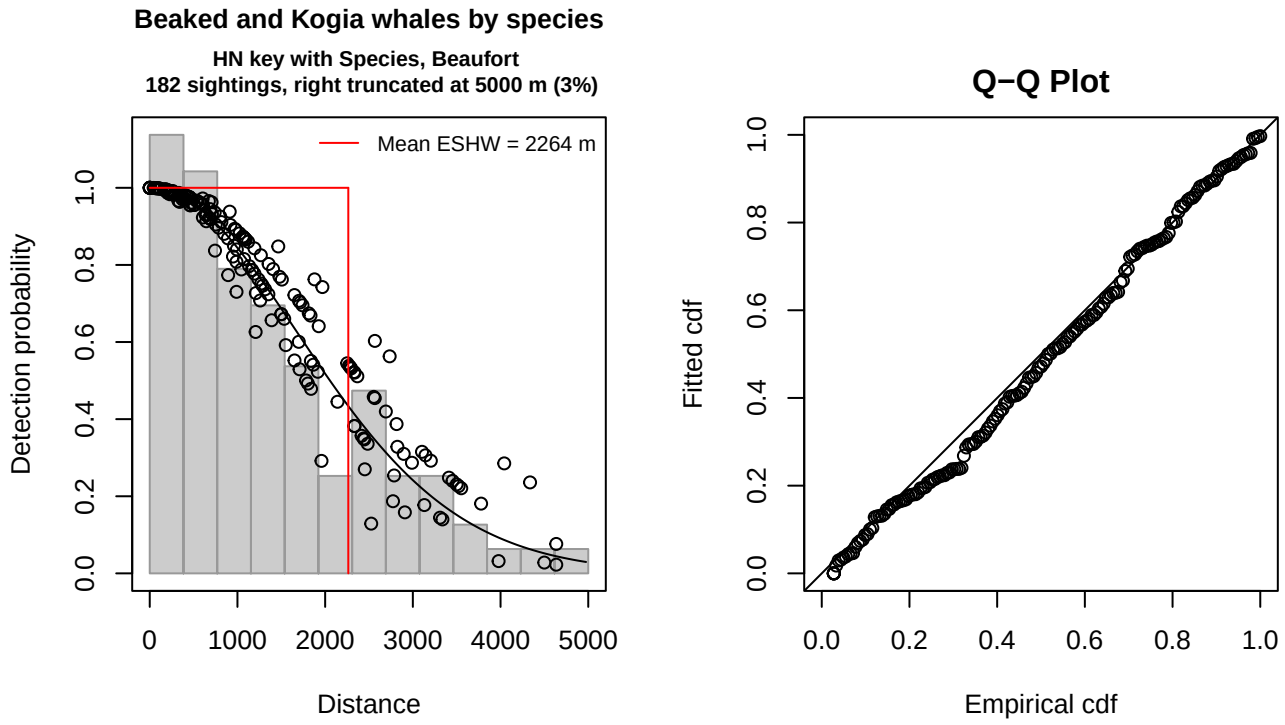

Figure 14: SEFSC detection function and Q-Q plot showing its goodness of fit.

Statistical output for this detection function:

```
Summary for ds object
Number of observations :  182
Distance range         :  0  -  5000
AIC                    :  2985.886

Detection function:
 Half-normal key function

Detection function parameters
Scale coefficient(s):
                                                        estimate
(Intercept)                                            7.4282169
OriginalScientificNameMesoplodon spp. and Unid. beaked whale  0.1940795
OriginalScientificNameZiphius or N. bottlenose         0.4163007
Beaufort3-4                                           -0.2991956
                                                              se
(Intercept)                                           0.08116764
```

```
OriginalScientificNameMesoplodon spp. and Unid. beaked whale 0.12604909
OriginalScientificNameZiphius or N. bottlenose               0.24124124
Beaufort3-4                                                  0.13661134

                        Estimate          SE         CV
Average p               0.4423162  0.02407533 0.05443013
N in covered region 411.4703239 32.09594942 0.07800307

Distance sampling Cramer-von Mises test (unweighted)
Test statistic = 0.128965  p = 0.460545
```

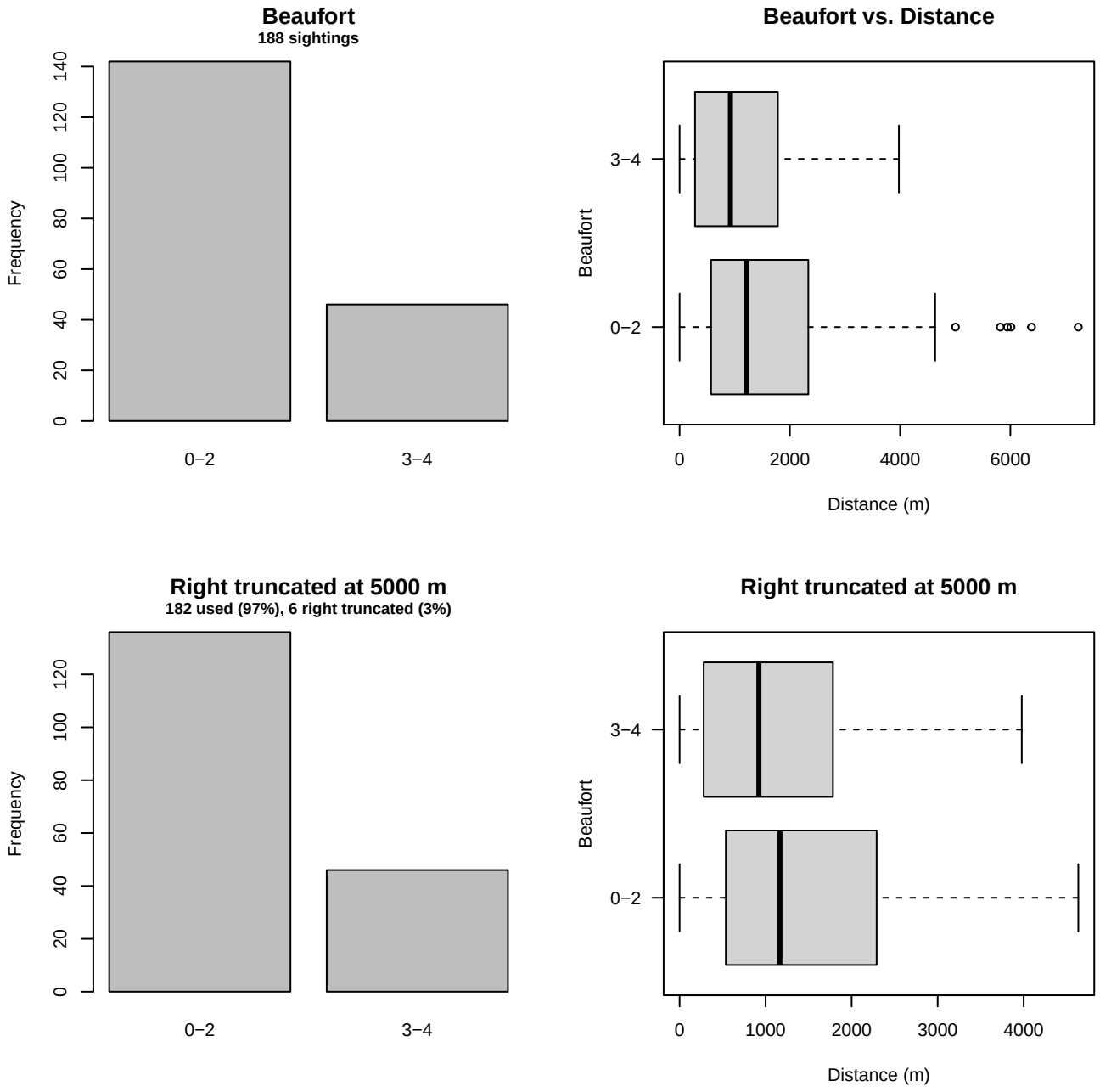

Figure 15: Distribution of the Beaufort covariate before (top row) and after (bottom row) observations were truncated to fit the SEFSC detection function.

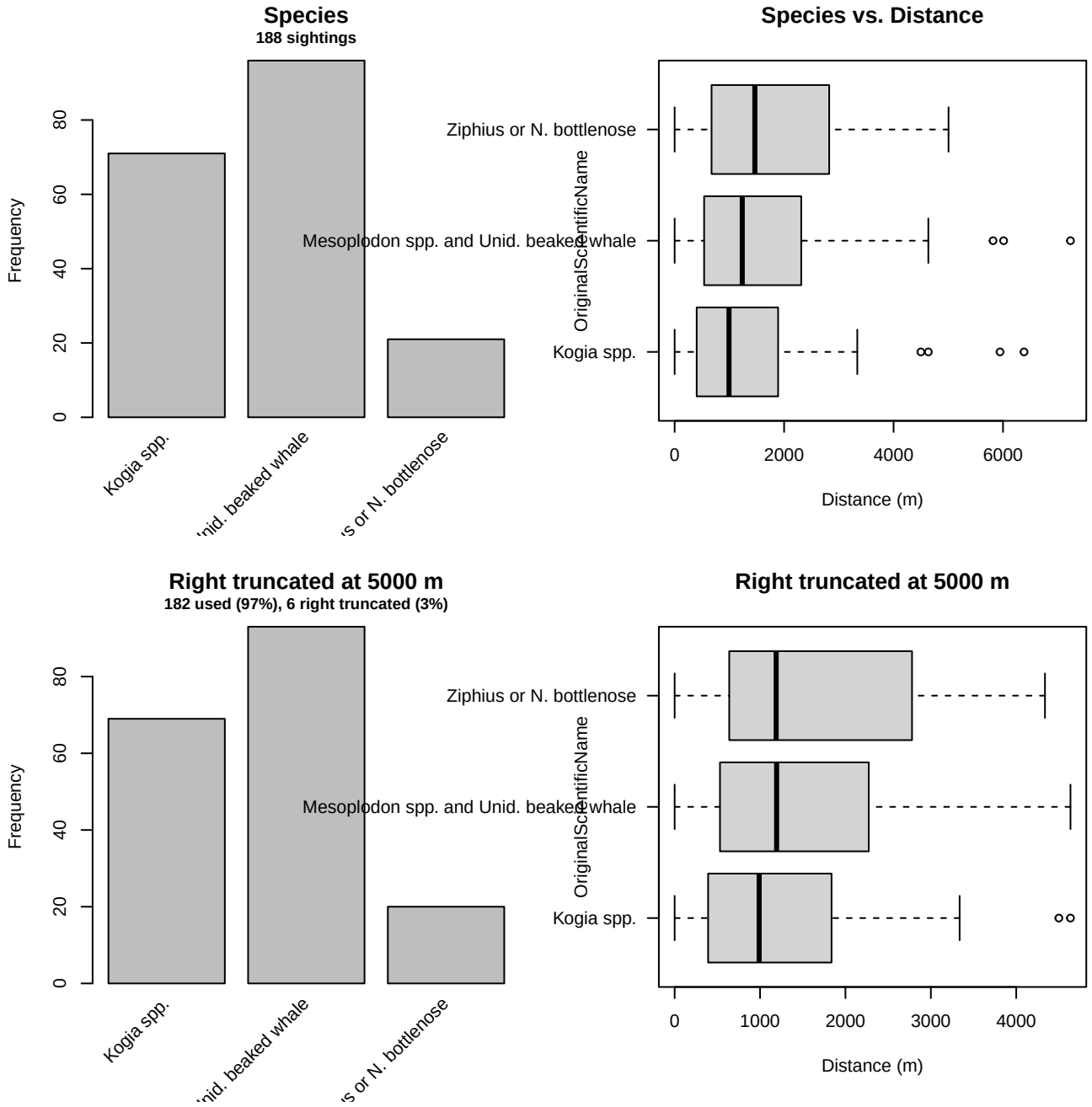

Figure 16: Distribution of the OriginalScientificName covariate before (top row) and after (bottom row) observations were truncated to fit the SEFSC detection function.

3 Bias Corrections

Density surface modeling methodology uses *distance sampling* (Buckland et al. 2001) to model the probability that an observer on a line transect survey will detect an animal given the perpendicular distance to it from the transect line. Distance sampling assumes that detection probability is 1 when perpendicular distance is 0. When this assumption is not met, detection probability is biased high, leading to an underestimation of density and abundance. This is known as the $g_0 < 1$ problem, where g_0 refers to the detection probability at distance 0. Modelers often try to address this problem by estimating g_0 empirically and dividing it into estimated density or abundance, thereby correcting those estimates to account for the animals that were presumed missed.

Two important sources of bias for visual surveys are known as *availability bias*, in which an animal was present on the transect line but impossible to detect, e.g. because it was under water, and *perception bias*, in which an animal was present and available but not noticed, e.g. because of its small size or cryptic coloration or behavior (Marsh and Sinclair 1989). Modelers often

estimate the influence of these two sources of bias on detection probability independently, yielding two estimates of g_0, hereafter referred to as g_{0A} and g_{0P}, and multiply them together to obtain a final, combined estimate: $g_0 = g_{0A}.g_{0P}$.

Our overall approach was to perform this correction on a per-observation basis, to have the flexibility to account for many factors such as platform type, surveyor institution, group size, group composition (e.g. singleton, mother-calf pair, or surface active group), and geographic location (e.g. feeding grounds vs. calving grounds). The level of complexity of the corrections varied by species according to the amount of information available, with North Atlantic right whale having the most elaborate corrections, derived from a substantial set of publications documenting its behavior, and various lesser known odontocetes having corrections based only on platform type (aerial or shipboard), derived from comparatively sparse information. Here we document the corrections used for dwarf and pygmy sperm whales.

3.1 Aerial Surveys

Very few Kogia were sighted on aerial surveys contributed by our collaborators. We found no perception bias estimates in the literature for Kogia sighted from aerial surveys, so we used beaked whales as a proxy. Palka et al. (2021) developed perception bias corrections for species guilds that included beaked whales using two team, mark recapture distance sampling (MRDS) methodology (Burt et al. 2014) for aerial surveys conducted in 2010-2017 by NOAA NEFSC and SEFSC during the AMAPPS program. These were the only extant perception bias estimates developed from aerial surveys used in our analysis, aside from estimates developed earlier by Palka and colleagues (Palka 2006; Palka et al. 2017). Those earlier efforts utilized older methods and less data than their 2021 analysis, so we applied the Palka et al. (2021) estimates to all aerial survey programs (Table 9).

We applied Palka's estimate for NEFSC to all programs other than SEFSC on the basis that those programs employed a similar visual scanning protocol that allowed observers to scan from the trackline up to the horizon, while SEFSC's protocol generally limited scanning only up to 50° from the trackline, resulting in a smaller effective strip width.

We caution that it is possible that perception bias was different on the other aerial programs, as they often used different aircraft, flew at different altitudes, and were staffed by different personnel. Of particular concern are that many programs flew Cessna 337 Skymasters, which had flat windows, while NOAA flew de Havilland Twin Otters, which had bubble windows, which likely afforded a better view of the transect line and therefore might have required less of a correction than the Skymasters. Correcting the other programs using NOAA's estimate as we have done is likely to yield less bias than leaving them uncorrected, but we urge all programs to undertake their own efforts to estimate perception bias, as resources allow.

We estimated availability bias corrections using the Laake et al. (1997) estimator and dive intervals reported by Palka et al. (2017) (Table 10). To estimate time in view, needed by the Laake estimator, we used results reported by Robertson et al. (2015), rescaled linearly for each survey program according to its target altitude and speed. We caution that Robertson's analysis was done for a de Havilland Twin Otter, which may have a different field of view than that of the other aircraft used here, which mainly comprised Cessna 337 Skymasters with flat windows but also a Partenavia P-68 with bubble windows (on the NYS-DEC/TT surveys). However, we note that McLellan et al. (2018) conducted a sensitivity analysis on the influence of the length of the "window of opportunity" to view beaked whales from a Cessna Skymaster on their final density estimates and found that they varied by only a few thousandths of an animal per kilometer when the window of opportunity more than doubled. Still, we urge additional program-specific research into estimation of availability bias.

To address the influence of group size on availability bias, we applied the group availability estimator of McLellan et al. (2018) on a per-observation basis. Following Palka et al. (2021), who also used that method, we assumed that individuals in the group dived asynchronously. The resulting g_{0A} corrections ranged from about 0.15 to 0.65 (Figure 17). We caution that the assumption of asynchronous diving can lead to an underestimation of density and abundance if diving is actually synchronous; see McLellan et al. (2018) for an exploration of this effect. However, if future research finds that this species conducts synchronous dives and characterizes the degree of synchronicity, the model can be updated to account for this knowledge.

Table 9: Perception bias corrections for dwarf and pygmy sperm whales applied to aerial surveys.

Surveys	Group Size	g_{0P}	g_{0P} Source
SEFSC	Any	0.86	Palka et al. (2021): SEFSC
All others	Any	0.62	Palka et al. (2021): NEFSC

Table 10: Surface and dive intervals for dwarf and pygmy sperm whales used to estimate availability bias corrections.

Surface Interval (s)	Dive Interval (s)	Source
78	654	Palka et al. (2017)

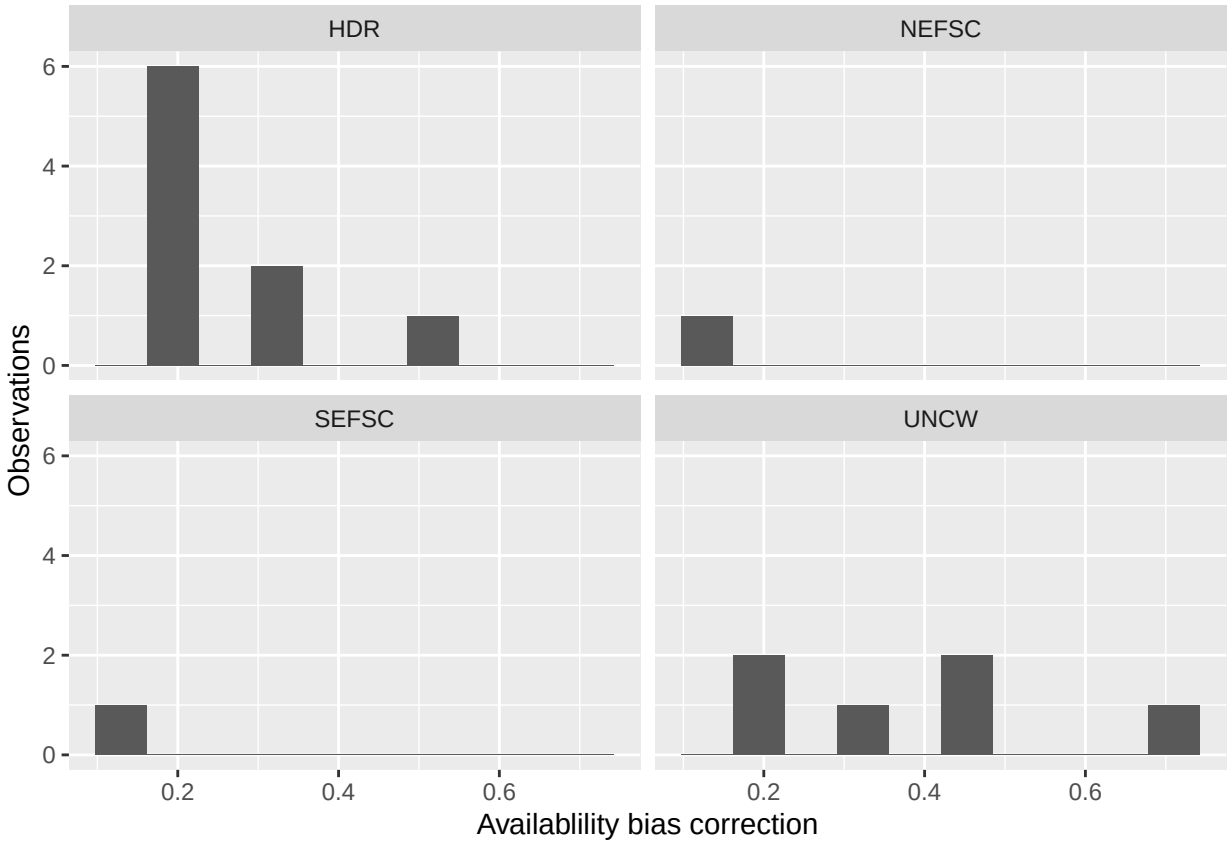

Figure 17: Availability bias corrections for dwarf and pygmy sperm whales for aerial surveys, by institution.

3.2 Shipboard Surveys

Most of the shipboard surveys in our analysis used high-power (25x150), pedestal-mounted binoculars. Similar to aerial surveys, Palka et al. (2021) developed perception bias corrections using two team, MRDS methodology (Burt et al. 2014) for high-power binocular surveys conducted in 2010-2017 by NOAA NEFSC and SEFSC during the AMAPPS program. In the case of NEFSC, the estimate was for a guild of beaked whales and Kogia species; in the case of SEFSC, the estimate was for Kogia only. These were the only extant perception bias estimates developed from high-power binocular surveys used in our analysis, aside from estimates developed earlier by Palka and colleagues (Palka 2006; Palka et al. 2017). Those earlier efforts utilized older methods and less data than their 2021 analysis, so we applied the Palka et al. (2021) estimates to all shipboard surveys that searched with high-power binoculars (Table 11).

There were no naked eye surveys for Kogia sp. used in this analysis.

Table 11: Perception and availability bias corrections for dwarf and pygmy sperm whales applied to shipboard surveys.

Surveys	Searching Method	Group Size	g_{0P}	g_{0P} Source	g_{0A}	g_{0A} Source
NEFSC	Binoculars	Any	0.42	Palka et al. (2021): NEFSC	0.54	Palka et al. (2017)
SEFSC	Binoculars	Any	0.48	Palka et al. (2021): SEFSC	0.54	Palka et al. (2017)

4 Density Model

The two extant species of Kogia, the dwarf sperm whale (Kogia sima) and the pygmy sperm whale (Kogia breviceps), are very difficult for observers to distinguish at sea and are cryptic in general, and difficult to sight except in the calmest sea states (Jefferson and Schiro 1997). Both species occur worldwide in tropical to temperate seas, generally in oceanic waters (Willis and Baird 1998; Bloodworth and Odell 2008; Waring 2013). Although pygmy sperm whales are considered a more temperate species, the habitats and diets of the two species overlap substantially (Staudinger et al. 2014). In the western Atlantic, Kogiid species sightings occur primarily over the continental slope and shelf break from Florida to Canada, possibly to feed on cephalopods, a staple of their diet (Bloodworth and Odell 2008).

In addition to being visibly difficult to distinguish, Kogiid species cannot be differentiated from one another acoustically at this time, however their narrow-band high frequency clicks can be distinguished from other species in deep offshore waters (Merkens et al. 2018). Hodge et al. (2018) reported Kogia detections from acoustic monitoring sites between Virginia and Florida and found that Kogia are more prevalent in this regions than visual surveys would suggest. Cohen et al. (2022) detected Kogia sp. clicks at 11 acoustic monitoring sites from Heezen Canynon in the north to Jacksonville in the south. The authors found that Kogia occurrence was predominant at the four sites in the South Atlantic Bight compared to the northern sites. They also noted a seasonal signal at the Gulf Stream site, with increased presence in the winter and spring compared to the summer and fall, but consistency across seasons at the other southern sites (Cohen et al. 2022). Kowarski et al. (2022) collected acoustic data at seven sites spanning Virginia to the Blake Escarpment between late 2017 and late 2020 using bottom-mounted autonomous recorders located at along the US Atlantic Outer Continental Shelf (OCS) in depths of 212–900 m. The authors reported Kogia clicks at all stations except Virginia Inter-Canyon (VAC) and Hatteras South (HAT) (Kowarski et al. 2022). The HAT station was located in less than 300m of water, whereas other studies (e.g., Hodge et al. (2018) and Cohen et al. (2022)), had recorders located in greater than 700 m depth, likely resulting in this difference in findings. Kogia clicks were present at Blake Escarpment (BLE) during almost every month of the three year recording period, and in Wilmington (WIL) and Savannah Deep (SAV) during a majority of months (Kowarski et al. 2022). Additionally, acoustic recordings off of Jackonville detected Kogia spp. clicks in 2014–2019 in all months of the year (Hodge et al. 2018; Cohen et al. 2022).

The large majority of sightings reported by the surveys included in our study reported "dwarf or pygmy sperm whale" as the taxonomic identification, and too few fully-identified sightings were reported to fit a habitat-based model for classifying the ambiguous observations. But given the apparent overlap in their habitats, we are uncertain that such an approach would be successful anyway. As such, we modeled both species as a guild, as NOAA has historically done (Mullin and Fulling 2003; Palka 2006). Given that there were only 5 sightings of Kogia prior to 1998 and ocean color covariates were unavailable for data before that year, we elected to model Kogia during the 1998-2019 survey period. We excluded 2020 from the models so that we could use "micronekton biomass, distance to eddies and kinetic energy covariates as candidates in the model. We found no definitive descriptions in the literature of seasonal movements by Kogia in the study area and a seasonal signal was only identified at one acoustic recording site in the Gulf Stream, as noted above (Cohen et al. 2022). However, given the spatial limitation of the recorder, we did not deem this a strong indication of seasonal movement. Accordingly, we fitted a year-round model to the entire study area and provided year-round mean abundance estimates rather than monthly estimates.

The Kogia model contained over 1 million km of segments with 152 total sightings of groups. Models fitted using contemporaneous predictors explained more deviance and had lower AIC and REML scores than the models fitted to the same segments using climatological covariates. A total of 5 covariates were retained in the top model (Table 12) (Figure 21). The retained covariates included depth, lower mesopelagic micronekton, sea surface salinity (SSS), distance to canyons and seamounts, and distance to eddies (any polarity). There was a positive relationship with depth, whereby more animals were predicted in greater depths. The relationship to lower mesopelagic micronekton showed an envelope, with a peak at mid ranges of biomass, but dropping off at the highest levels. There was a negative relationship to sea surface salinity, primarily just delineating the offshore range of Kogia. Distance to canyons and seamounts had a positive relationship with fewer animals predicted close to canyons and seamounts, and finally distance to eddies showed a peak between 0 and 200 km from eddies.

4.1 Final Model

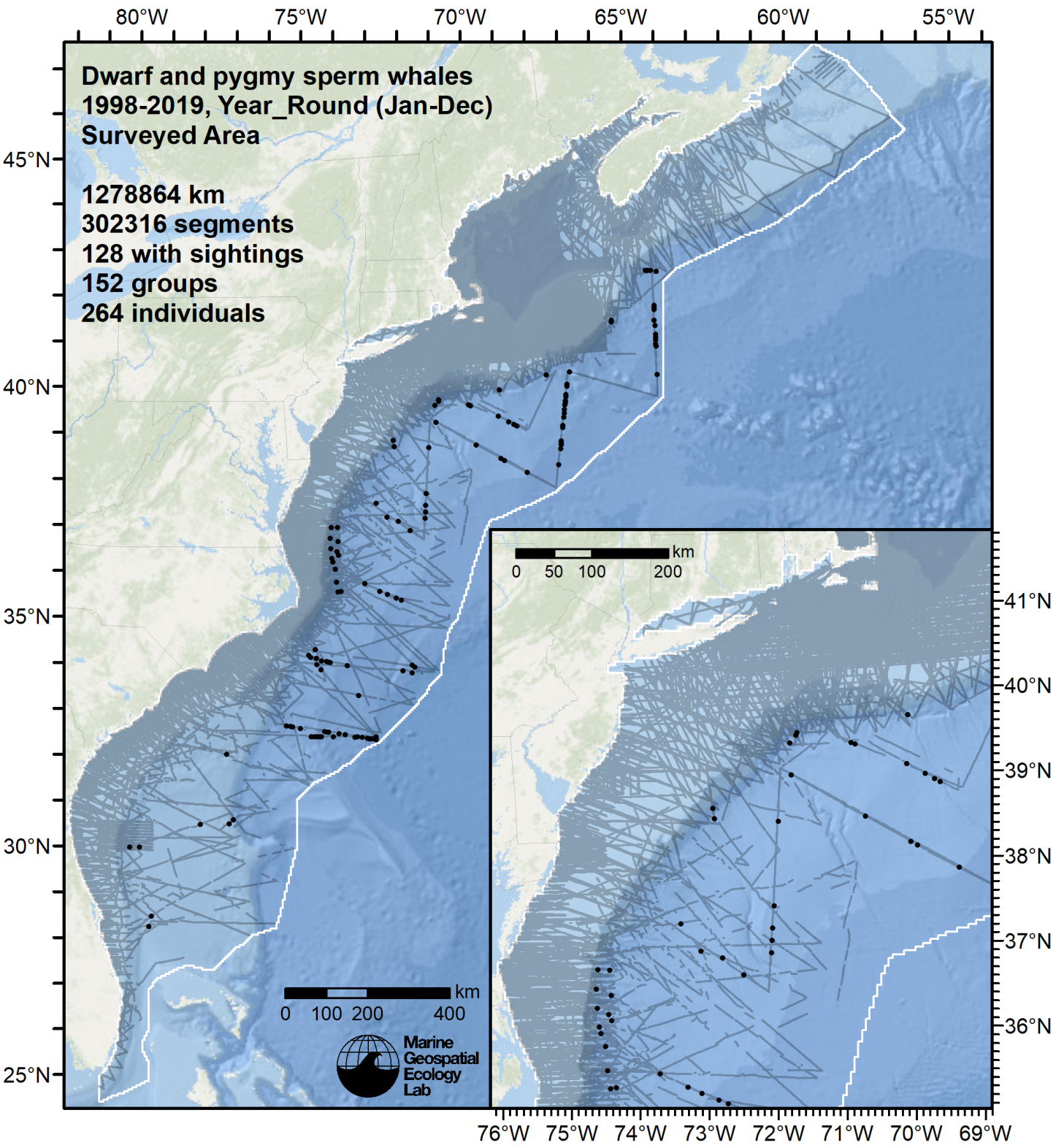

Figure 18: Survey segments used to fit the model. Black points indicate segments with observations.

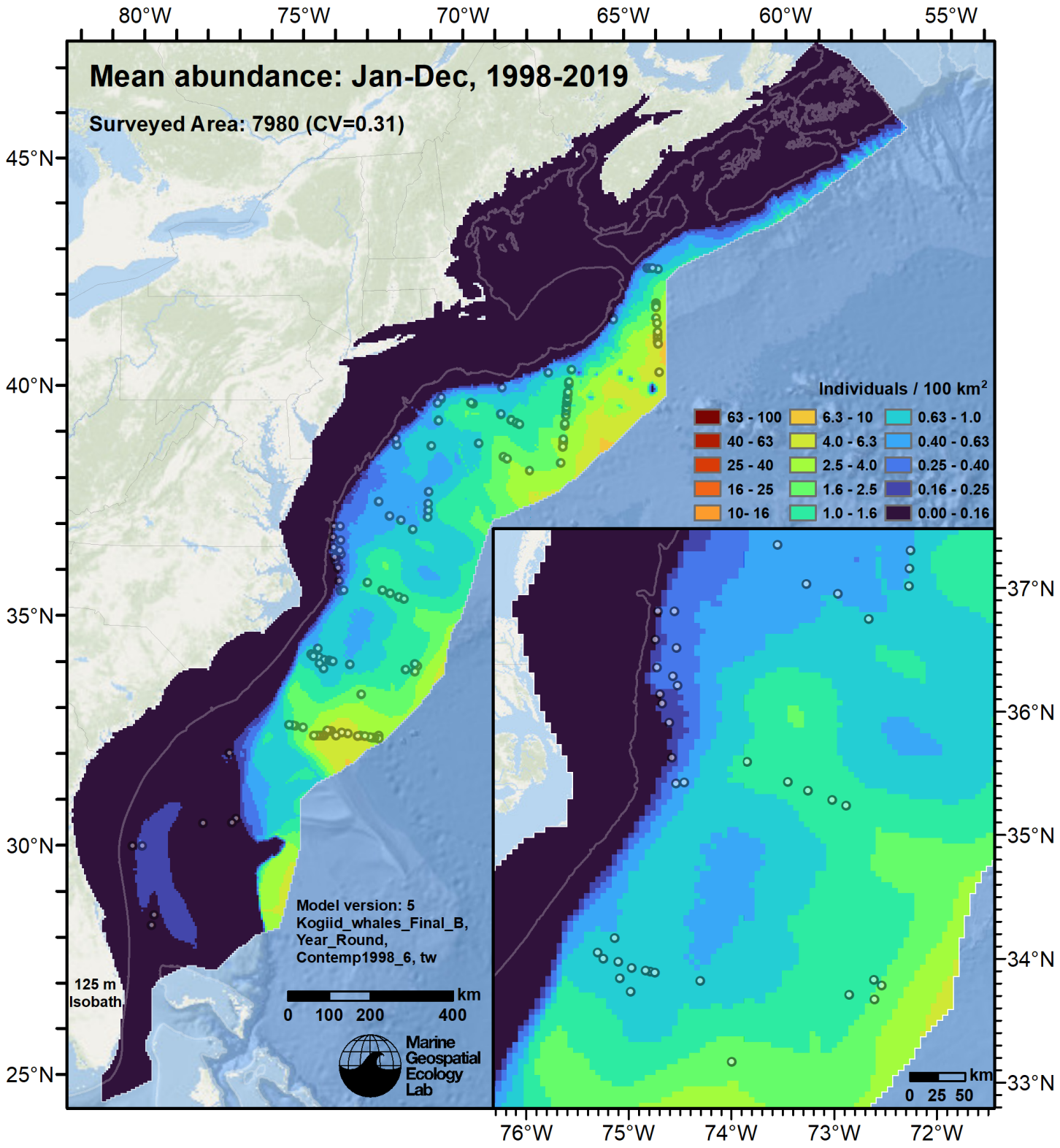

Figure 19: Dwarf and pygmy sperm whales mean density for the indicated period, as predicted by the model. Open circles indicate segments with observations. Mean total abundance and its coefficient of variation (CV) are given in the subtitle. Variance was estimated with the analytic approach given by Miller et al. (2022), Appendix S1, and accounts both for uncertainty in model parameter estimates and for seasonal and interannual variability in dynamic covariates.

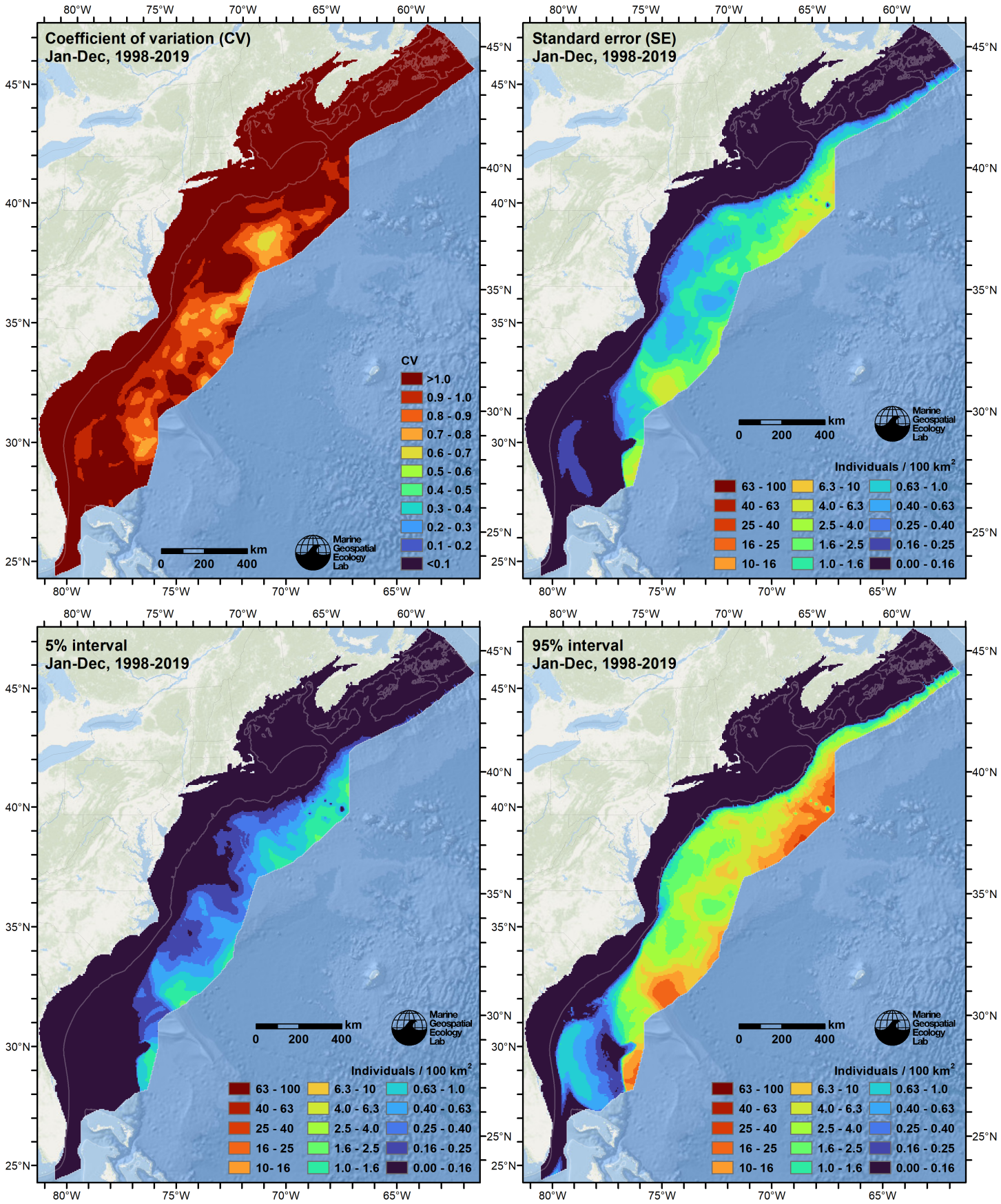

Figure 20: Uncertainty statistics for the dwarf and pygmy sperm whales mean density surface (Figure 19) predicted by the model. Variance was estimated with the analytic approach given by Miller et al. (2022), Appendix S1, and accounts both for uncertainty in model parameter estimates and for seasonal and interannual variability in dynamic covariates.

Statistical output for this model:

```
Family: Tweedie(p=1.178)
Link function: log

Formula:
IndividualsCorrected ~ offset(log(SegmentArea)) + s(log10(pmax(10,
    Depth)), bs = "ts") + s(log10(pmax(0.01, pmin(MnkLMeso, 5))),
    bs = "ts") + s(pmax(31, SSS_HYCOM), bs = "ts") + s(pmin(I(DistToCanOrSmt/1000),
    700), bs = "ts") + s(pmin(I(DistToEddy/1000), 350), bs = "ts")

Parametric coefficients:
            Estimate Std. Error t value Pr(>|t|)
(Intercept)   -39.97      10.47  -3.818 0.000134 ***
---
Signif. codes:  0 '***' 0.001 '**' 0.01 '*' 0.05 '.' 0.1 ' ' 1

Approximate significance of smooth terms:
                                        edf Ref.df      F  p-value
s(log10(pmax(10, Depth)))             2.923      9 17.736  < 2e-16 ***
s(log10(pmax(0.01, pmin(MnkLMeso, 5)))) 2.569      9  2.477 6.62e-06 ***
s(pmax(31, SSS_HYCOM))                1.024      9  1.731 4.87e-05 ***
s(pmin(I(DistToCanOrSmt/1000), 700))  1.015      9  2.445 1.43e-06 ***
s(pmin(I(DistToEddy/1000), 350))      4.560      9  5.242  < 2e-16 ***
---
Signif. codes:  0 '***' 0.001 '**' 0.01 '*' 0.05 '.' 0.1 ' ' 1

R-sq.(adj) =  0.048   Deviance explained = 55.5%
-REML = 1044.1  Scale est. = 14.367    n = 302316

Method: REML   Optimizer: outer newton
full convergence after 26 iterations.
Gradient range [-0.0005711941,0.0009008833]
(score 1044.051 & scale 14.36679).
Hessian positive definite, eigenvalue range [0.2313462,852.9864].
Model rank =  46 / 46

Basis dimension (k) checking results. Low p-value (k-index<1) may
indicate that k is too low, especially if edf is close to k'.

                                        k'  edf k-index p-value
s(log10(pmax(10, Depth)))             9.00 2.92    0.63  <2e-16 ***
s(log10(pmax(0.01, pmin(MnkLMeso, 5)))) 9.00 2.57    0.76  <2e-16 ***
s(pmax(31, SSS_HYCOM))                9.00 1.02    0.94   0.005 **
s(pmin(I(DistToCanOrSmt/1000), 700))  9.00 1.02    0.84  <2e-16 ***
s(pmin(I(DistToEddy/1000), 350))      9.00 4.56    0.91  <2e-16 ***
---
Signif. codes:  0 '***' 0.001 '**' 0.01 '*' 0.05 '.' 0.1 ' ' 1
```

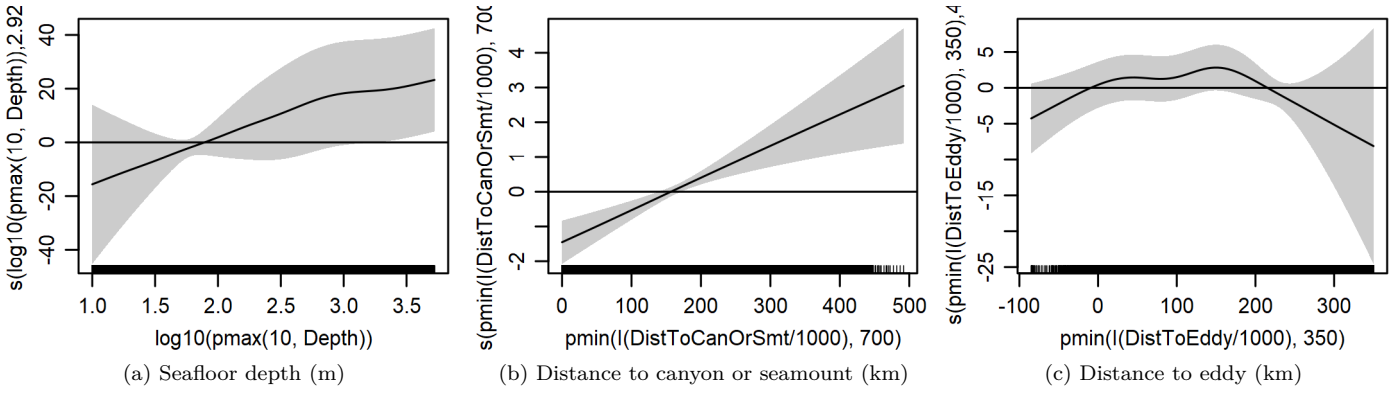

(a) Seafloor depth (m) (b) Distance to canyon or seamount (km) (c) Distance to eddy (km)

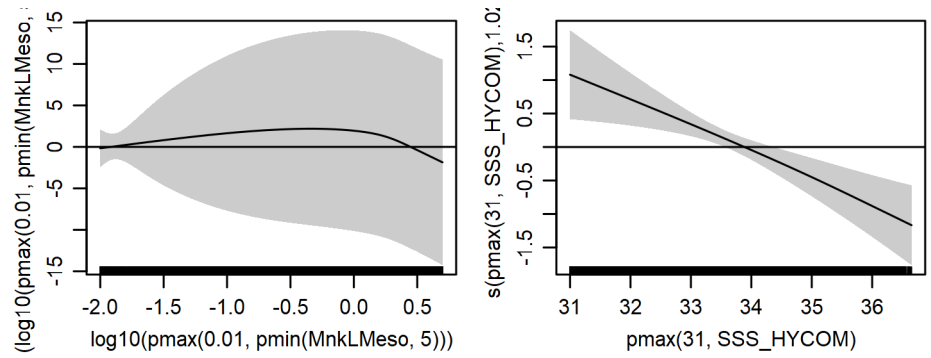

(d) Lower mesopelagic micronekton biomass (g m^{-2}) (e) Sea surface salinity (PSU)

Figure 21: Functional plots for the final model. Transforms and other treatments are indicated in axis labels. *log10* indicates the covariate was $\log_{10}$ transformed. *pmax* and *pmin* indicate the covariate's minimum and maximum values, respectively, were Winsorized to the values shown. Winsorization was used to prevent runaway extrapolations during prediction when covariates exceeded sampled ranges, or for ecological reasons, depending on the covariate. */1000* indicates meters were transformed to kilometers for interpretation convenience.

Table 12: Covariates used in the final model.

Covariate	Description
Depth	Depth (m) of the seafloor, from SRTM30_PLUS (Becker et al. (2009))
DistToCanOrSmt	Distance (km) to the closest submarine canyon or seamount, derived from the Harris et al. (2014) geomorphology
DistToEddy	Monthly mean distance (km) to the edge of the closest mesoscale eddy of any polarity and age, derived with MGET (Roberts et al. (2010)) from the Aviso Mesoscale Eddy Trajectories Atlas (META2.0), produced by SSALTO/DUACS and distributed by AVISO+ (https://aviso.altimetry.fr) with support from CNES, in collaboration with Oregon State University with support from NASA, using the method of Schlax and Chelton (2016), based on Chelton et al. (2011)
MnkLMeso	Monthly mean micronekton biomass available in the lower mesopelagic zone, expressed as wet weight (g m^{-2}), from SEAPODYM (Lehodey et al. (2008); Lehodey et al. (2015)), provided by E.U. Copernicus Marine Service. doi: 10.48670/moi-00020. Computed as the sum of the SEAPODYM mnkc_lmeso, mnkc_mlmeso, and mnkc_hmlmeso variables.
SSS_HYCOM	Monthly mean sea surface salinity (PSU) from the HYCOM GOFS 3.1 1/12° ocean model (Chassignet et al. (2009))

4.2 Diagnostic Plots

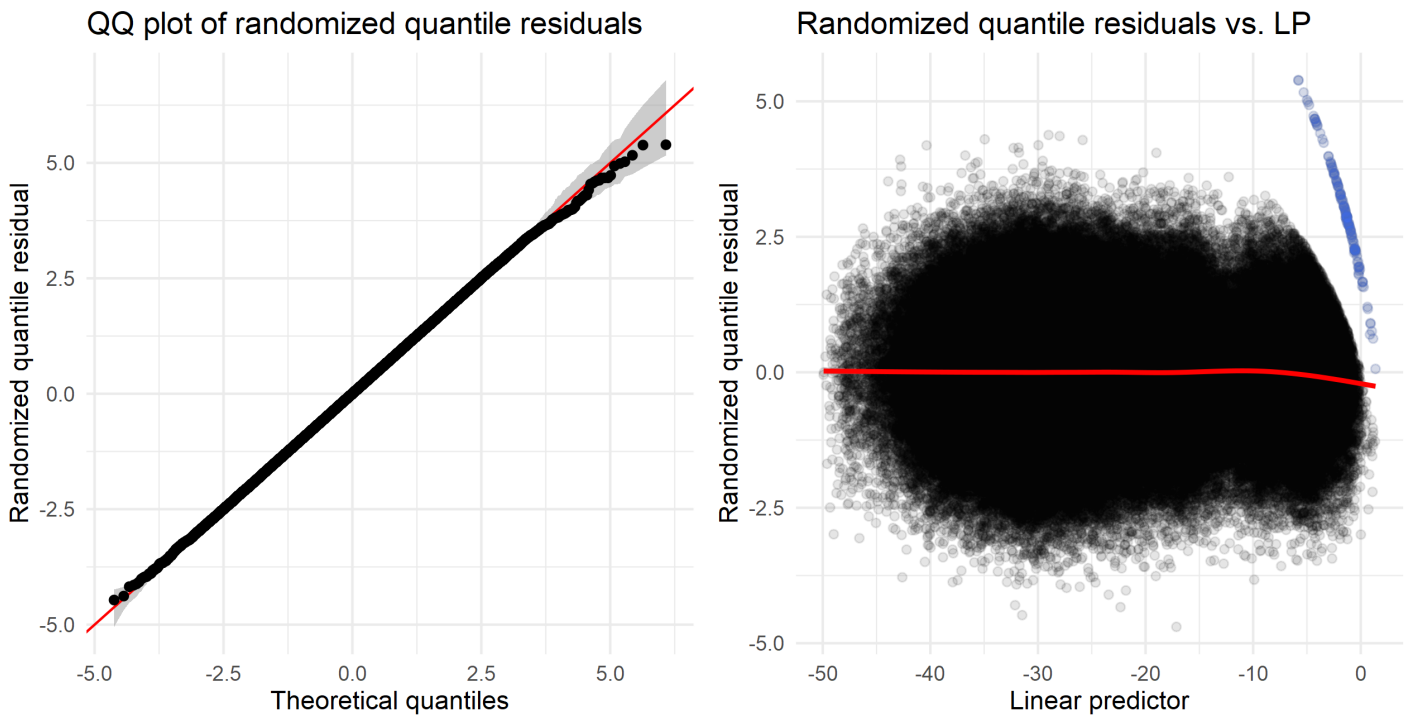

Figure 22: Residual plots for the final model.

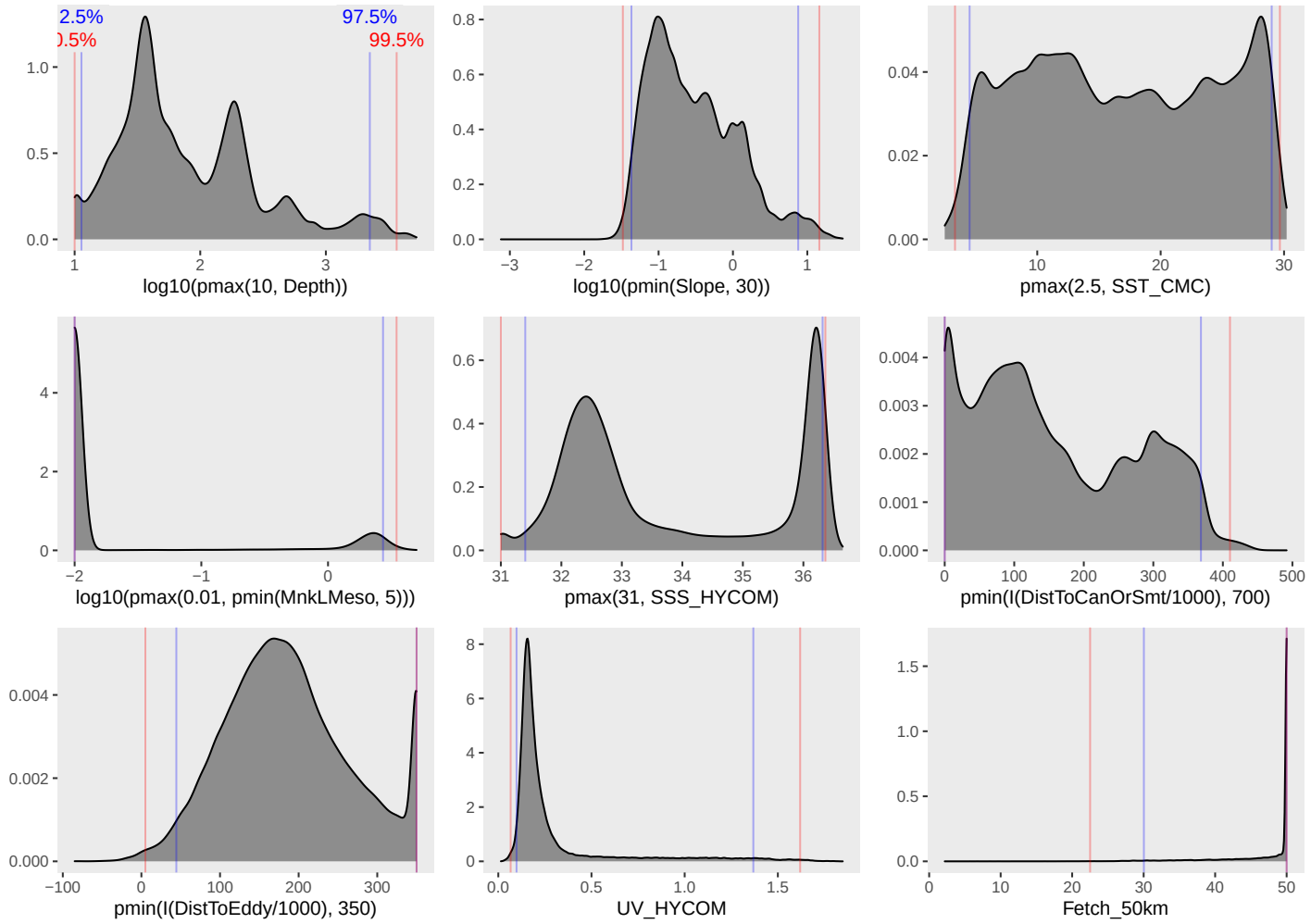

Figure 23: Density histograms showing the distributions of the covariates considered during the final model selection step. The final model may have included only a subset of the covariates shown here (see Figure 21), and additional covariates may have been considered in preceding selection steps. Red and blue lines enclose 99% and 95% of the distributions, respectively. Transforms and other treatments are indicated in axis labels. *log10* indicates the covariate was $\log_{10}$ transformed. *pmax* and *pmin* indicate the covariate's minimum and maximum values, respectively, were Winsorized to the values shown. Winsorization was used to prevent runaway extrapolations during prediction when covariates exceeded sampled ranges, or for ecological reasons, depending on the covariate. */1000* indicates meters were transformed to kilometers for interpretation convenience.

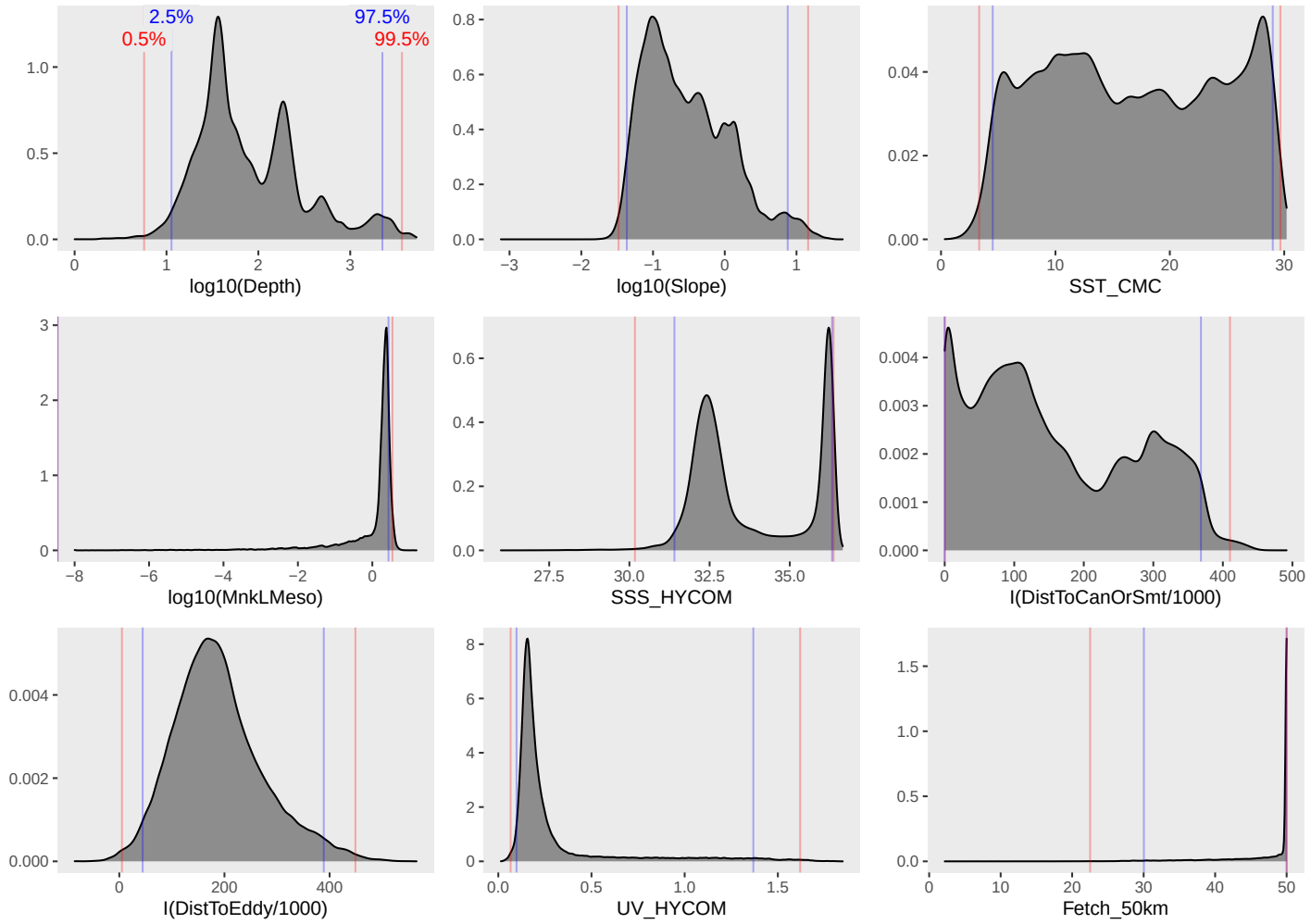

Figure 24: Density histograms shown in Figure 23 replotted without Winsorization, to show the full range of sampling represented by survey segments.

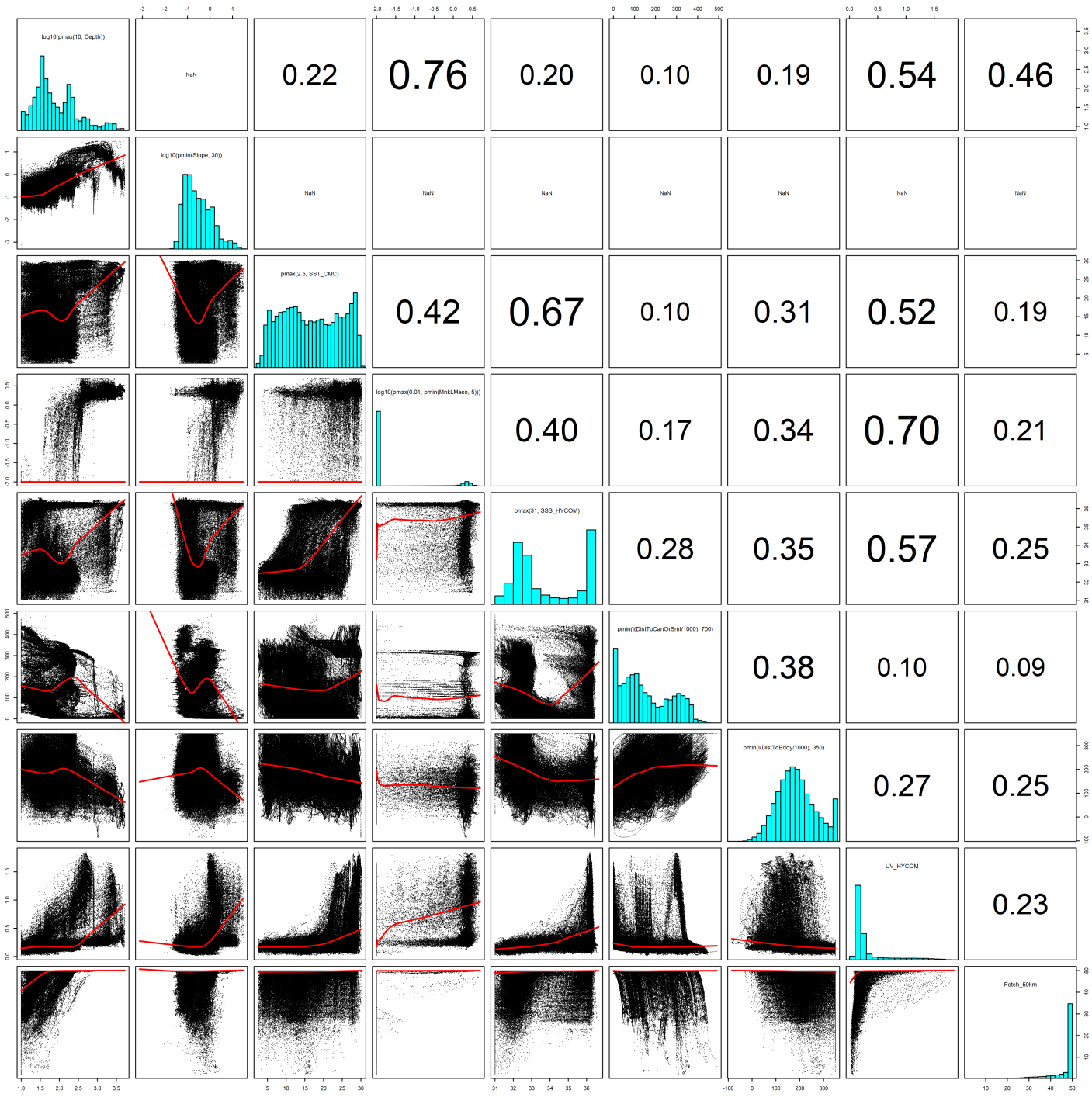

Figure 25: Scatterplot matrix of the covariates considered during the final model selection step. The final model may have included only a subset of the covariates shown here (see Figure 21), and additional covariates may have been considered in preceding selection steps. Covariates are transformed and Winsorized as shown in Figure 23. This plot is used to check simple correlations between covariates (via pairwise Pearson coefficients above the diagonal) and visually inspect for concurvity (via scatterplots and red lowess curves below the diagonal).

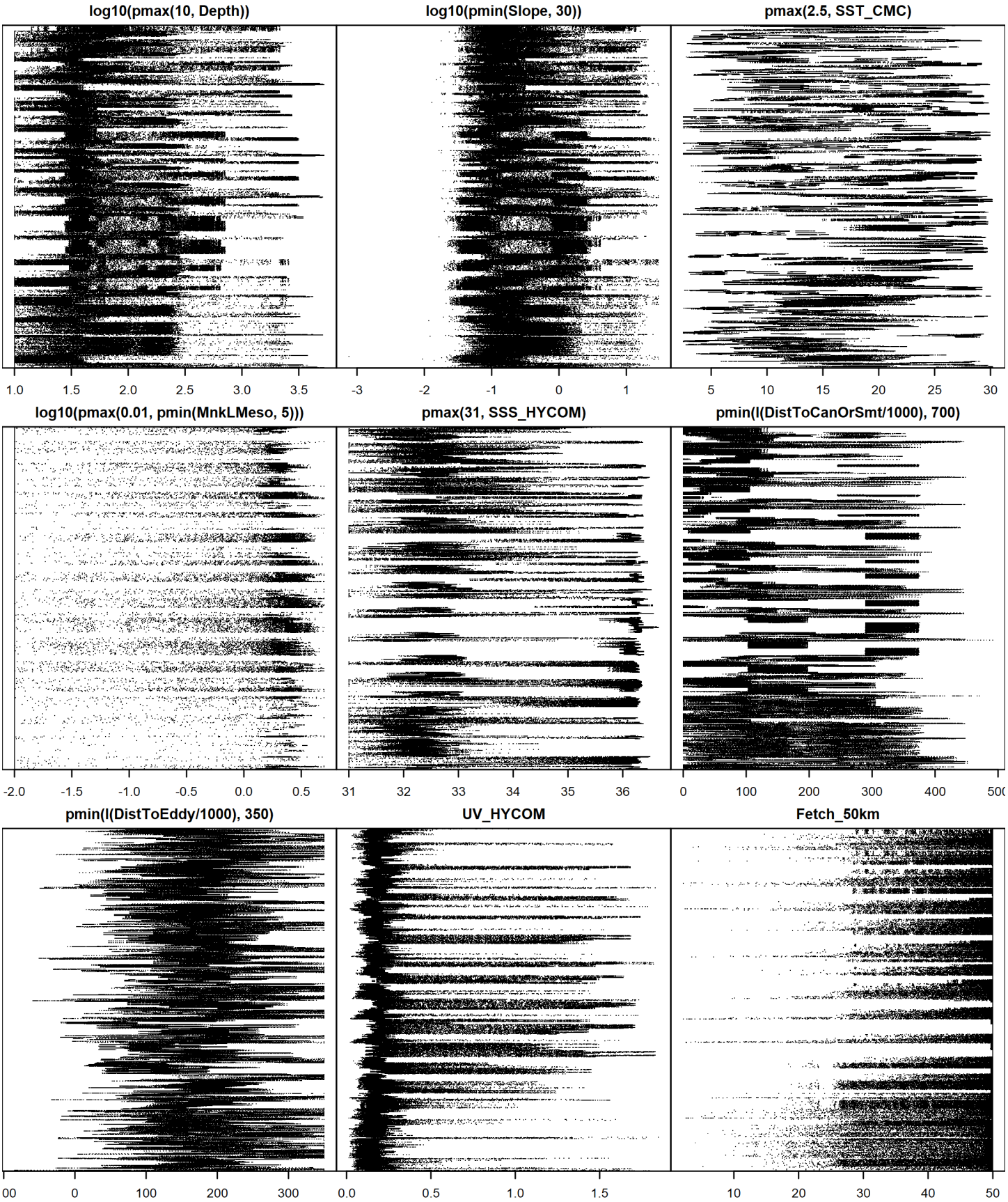

Figure 26: Dotplot of the covariates considered during the final model selection step. The final model may have included only a subset of the covariates shown here (see Figure 21), and additional covariates may have been considered in preceding selection steps. Covariates are transformed and Winsorized as shown in Figure 23. This plot is used to check for suspicious patterns and outliers in the data. Points are ordered vertically by segment ID, sequentially in time.

4.3 Extrapolation Diagnostics

4.3.1 Univariate Extrapolation

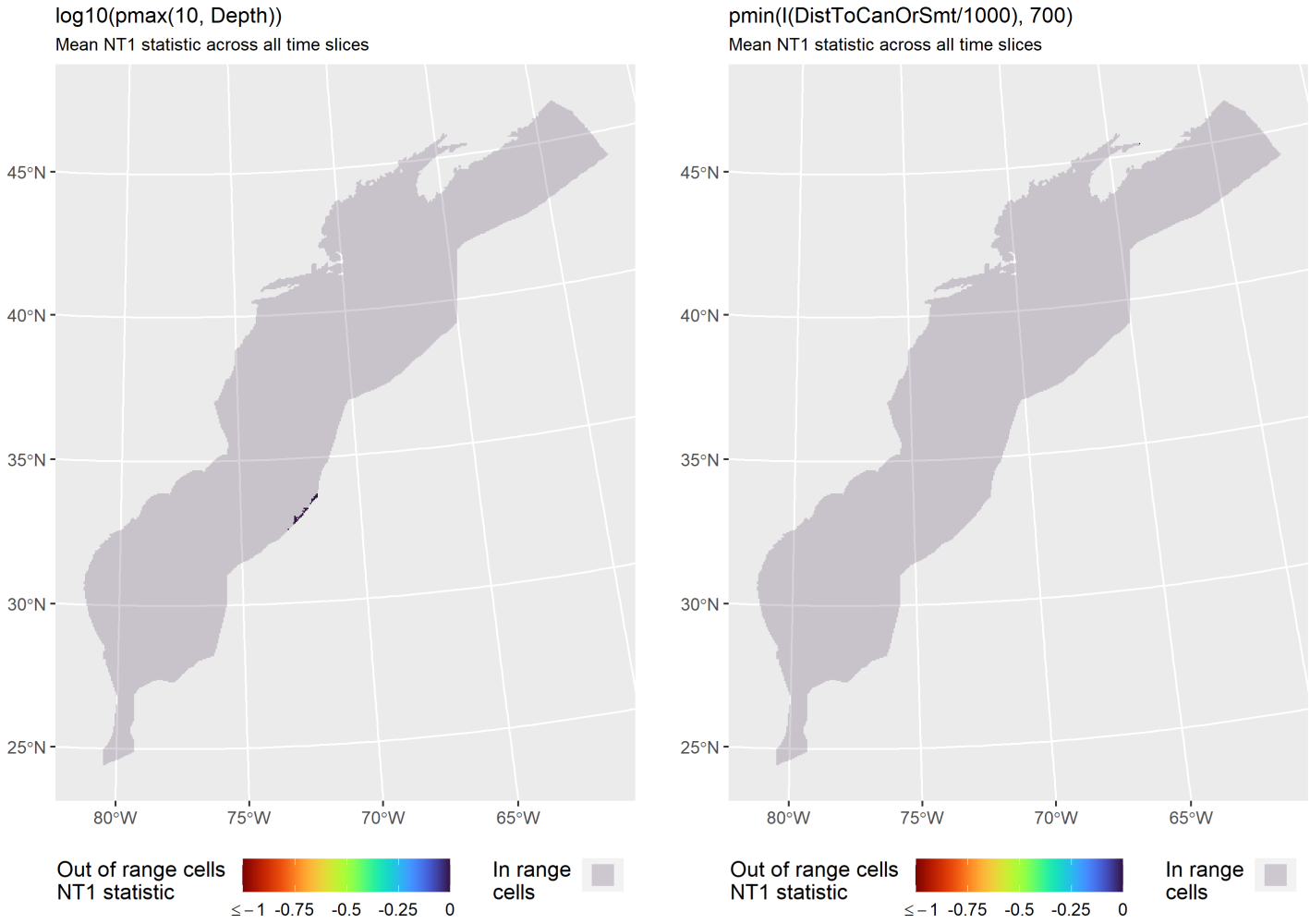

(a) Depth covariate

(b) DistToCanOrSmt covariate

Figure 27: NT1 statistic (Mesgaran et al. (2014)) for static covariates used in the model. Areas outside the sampled range of a covariate appear in color, indicating univariate extrapolation of that covariate occurred there. Areas within the sampled range appear in gray, indicating it did not occur.

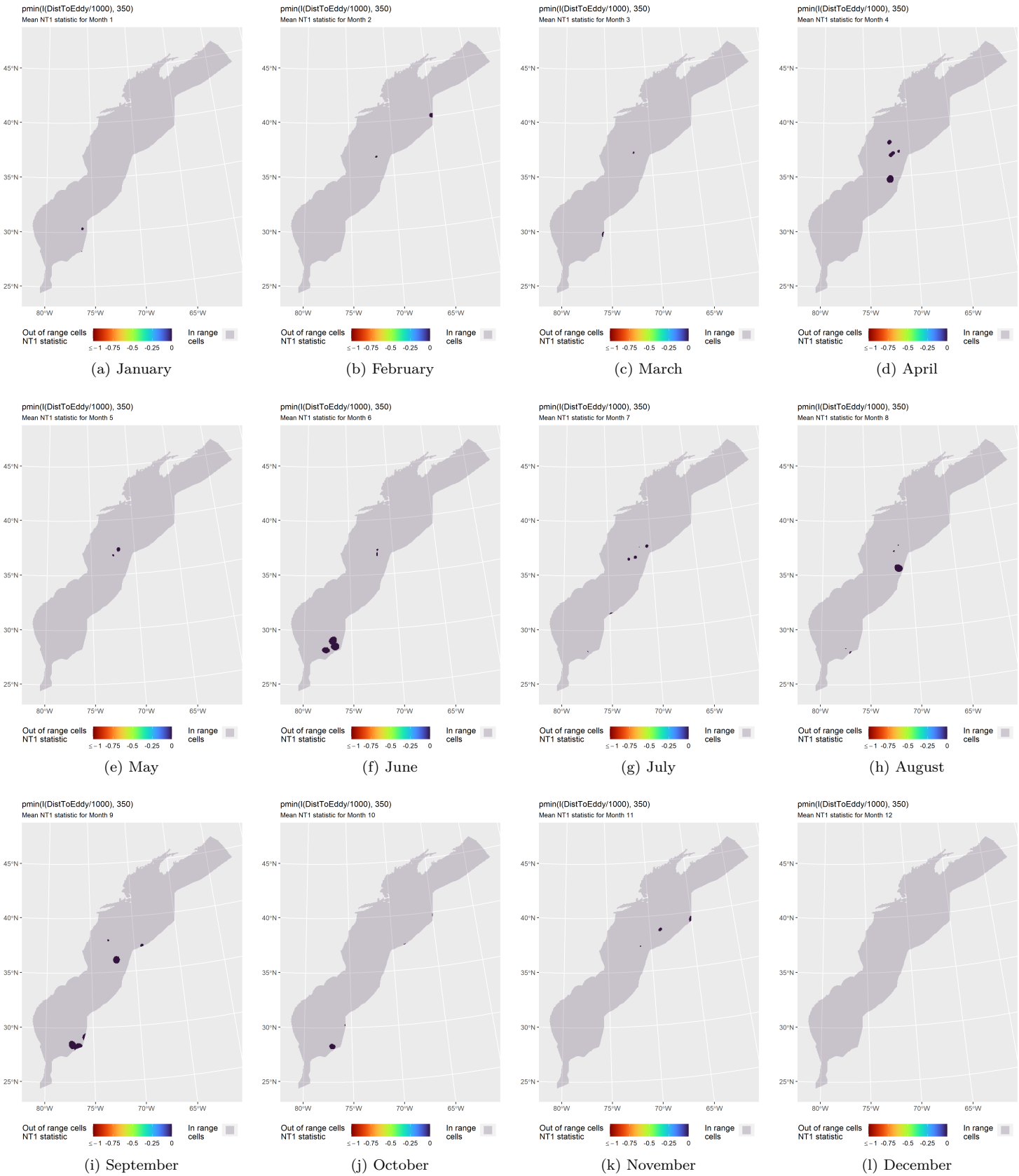

(a) January (b) February (c) March (d) April

(e) May (f) June (g) July (h) August

(i) September (j) October (k) November (l) December

Figure 28: NT1 statistic (Mesgaran et al. (2014)) for the DistToEddy covariate in the model. Areas outside the sampled range of a covariate appear in color, indicating univariate extrapolation of that covariate occurred there during the month. Areas within the sampled range appear in gray, indicating it did not occur.

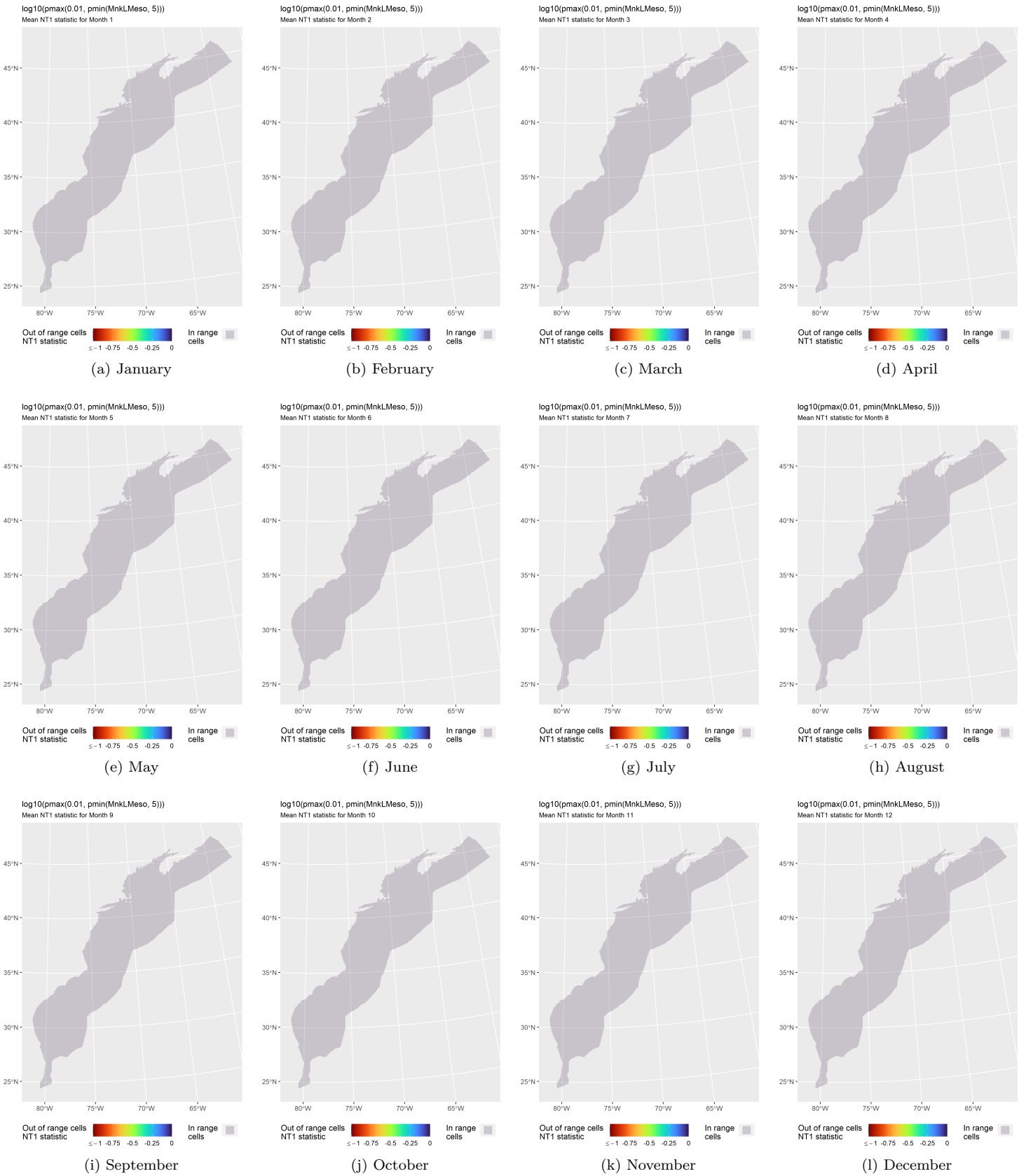

(a) January (b) February (c) March (d) April

(e) May (f) June (g) July (h) August

(i) September (j) October (k) November (l) December

Figure 29: NT1 statistic (Mesgaran et al. (2014)) for the MnkLMeso covariate in the model. Areas outside the sampled range of a covariate appear in color, indicating univariate extrapolation of that covariate occurred there during the month. Areas within the sampled range appear in gray, indicating it did not occur.

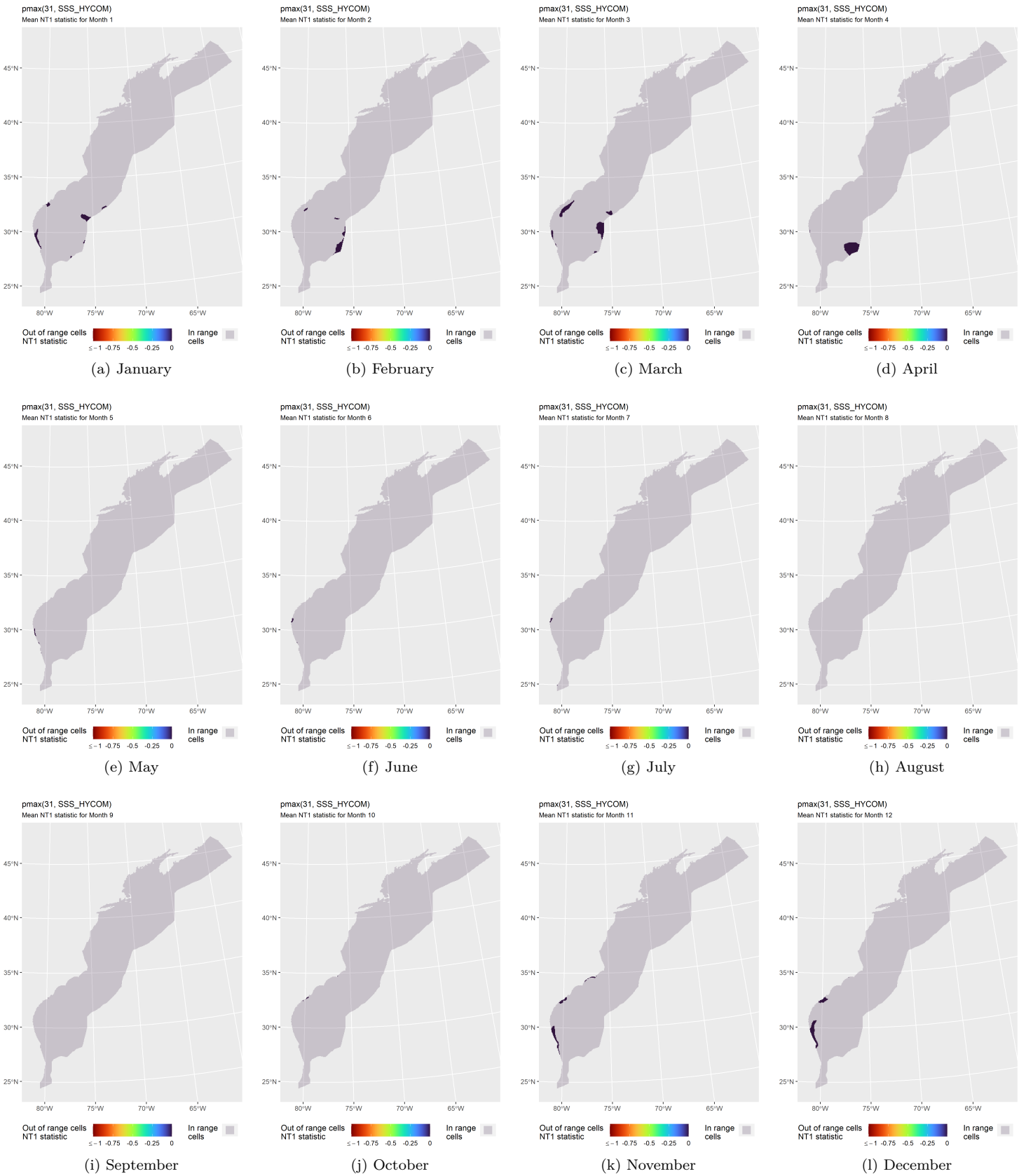

(a) January (b) February (c) March (d) April

(e) May (f) June (g) July (h) August

(i) September (j) October (k) November (l) December

Figure 30: NT1 statistic (Mesgaran et al. (2014)) for the SSS_HYCOM covariate in the model. Areas outside the sampled range of a covariate appear in color, indicating univariate extrapolation of that covariate occurred there during the month. Areas within the sampled range appear in gray, indicating it did not occur.

4.3.2 Multivariate Extrapolation

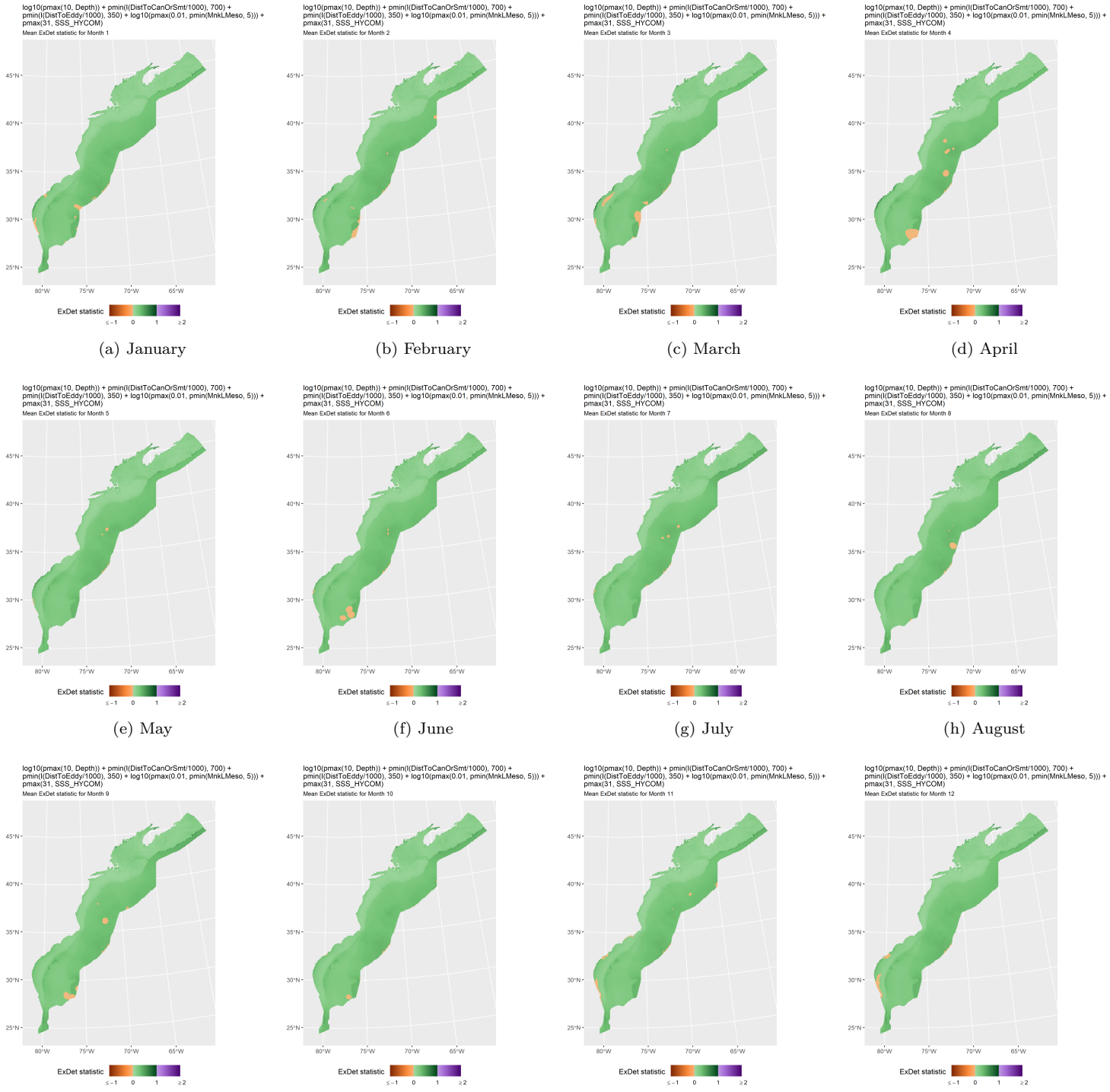

(a) January (b) February (c) March (d) April

(e) May (f) June (g) July (h) August

(i) September (j) October (k) November (l) December

Figure 31: ExDet statistic (Mesgaran et al. (2014)) for all of the covariates used in the model. Areas in orange (ExDet < 0) required univariate extrapolation of one or more covariates (see previous section). Areas in purple (ExDet > 1), did not require univariate extrapolation but did require multivariate extrapolation, by virtue of having novel combinations of covariates not represented in the survey data, according to the NT2 statistic (Mesgaran et al. (2014)). Areas in green ($0 \geq$ ExDet ≤ 1) did not require either type of extrapolation.

5 Predictions

Based on our evaluation of this model in the context of what is known of this species (see Section 4), we summarized its predictions into single, year-round climatological density and uncertainty surfaces (Figure 33). To illustrate the seasonal dynamics that result when predictions are summarized monthly instead, we included monthly mean abundances (Figure 32, Table 13), but to avoid confusion we did not include monthly maps in this report. They are available from us on request, but we recommend the year-round map be used for decision-making purposes, as discussed in Section 6.

5.1 Summarized Predictions

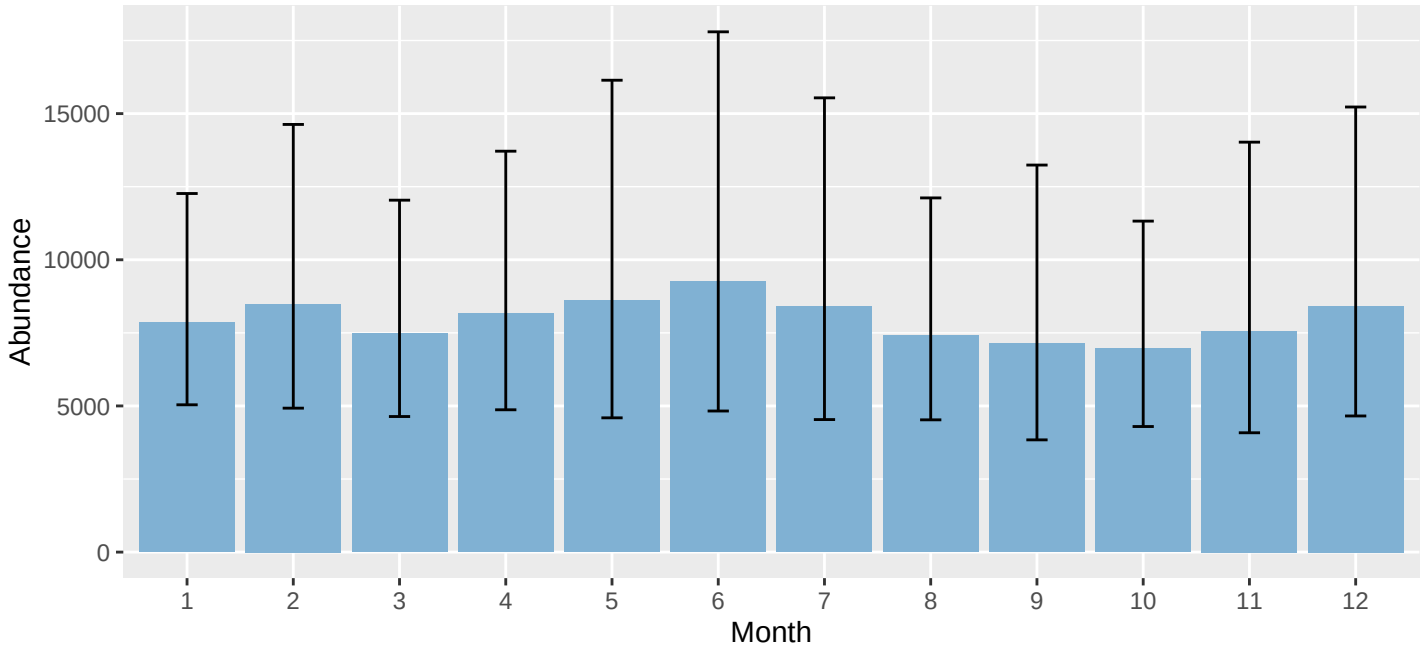

Figure 32: Mean monthly abundance for the prediction area for 1998-2019. Error bars are a 95% interval, made with a log-normal approximation using the prediction's CV. The CV was estimated with the analytic approach given by Miller et al. (2022), Appendix S1, and accounts both for uncertainty in model parameter estimates and for temporal variability in dynamic covariates.

Table 13: Mean monthly abundance and density for the prediction area for 1998-2019. CV and intervals estimated as described for the previous figure.

Month	Abundance	CV	95% Interval	Area (km^2)	Density (individuals / 100 km^2)
1	7,863	0.230	5,040 - 12,267	1,272,925	0.618
2	8,488	0.283	4,925 - 14,629	1,272,925	0.667
3	7,472	0.247	4,638 - 12,039	1,272,925	0.587
4	8,171	0.269	4,869 - 13,715	1,272,925	0.642
5	8,611	0.329	4,593 - 16,141	1,272,925	0.676
6	9,268	0.342	4,827 - 17,797	1,272,925	0.728
7	8,393	0.322	4,534 - 15,538	1,272,925	0.659
8	7,404	0.255	4,525 - 12,116	1,272,925	0.582
9	7,130	0.324	3,840 - 13,240	1,272,925	0.560
10	6,974	0.251	4,296 - 11,323	1,272,925	0.548
11	7,566	0.323	4,083 - 14,023	1,272,925	0.594
12	8,421	0.309	4,657 - 15,226	1,272,925	0.662

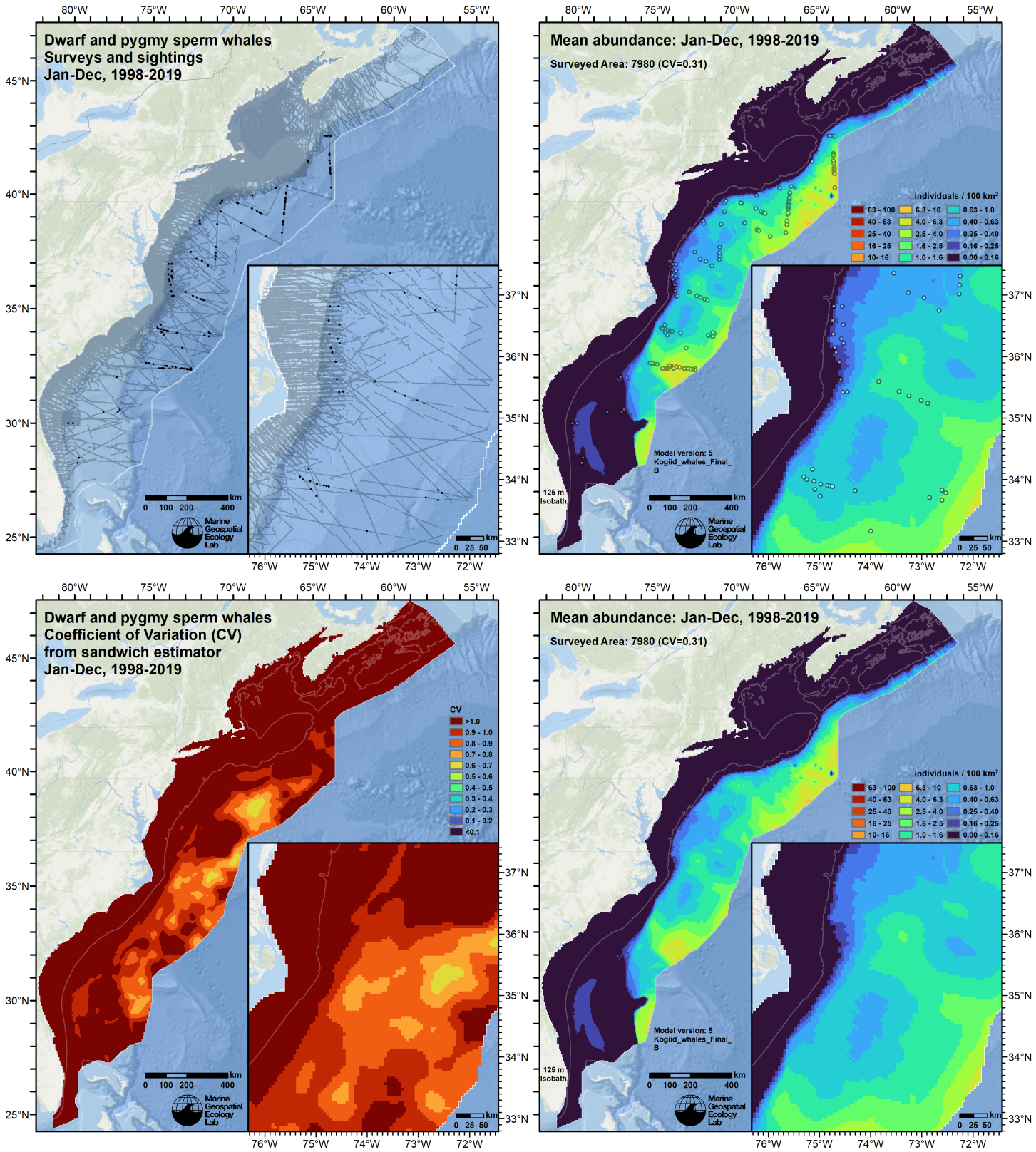

Figure 33: Survey effort and observations (top left), predicted density with observations (top right), predicted density without observations (bottom right), and coefficient of variation of predicted density (bottom left), for the given era. Variance was estimated with the analytic approach given by Miller et al. (2022), Appendix S1, and accounts both for uncertainty in model parameter estimates and for temporal variability in dynamic covariates.

5.2 Abundance Comparisons

5.2.1 NOAA Stock Assessment Report

Table 14: Comparison of regional abundance estimates from the 2021 NOAA Stock Assessment Report (SAR) (Hayes et al. (2022)) to estimates from this density model extracted from roughly comparable zones (Figure 34 below). The SAR estimates were based on a single year of surveying, while the model estimates were taken from the multi-year mean density surfaces we provide to model users (Section 5.1).

2021 Stock Assessment Report			Density Model		
Month/Year	Area	N_{est}	Period	Zone	Abundance
Jun-Aug 2016	Central Virginia to lower Bay of Fundy[a]	4,548	Year-Round 1998-2019	NEFSC	3,846
Jun-Aug 2016	Florida to central Virginia[b]	3,202	Year-Round 1998-2019	SEFSC	3,739
Jun-Aug 2016	Total	7,750	Year-Round 1998-2019	Total	7,585

[a] Estimate originally from Palka (2020).
[b] Estimate originally from Garrison (2020).

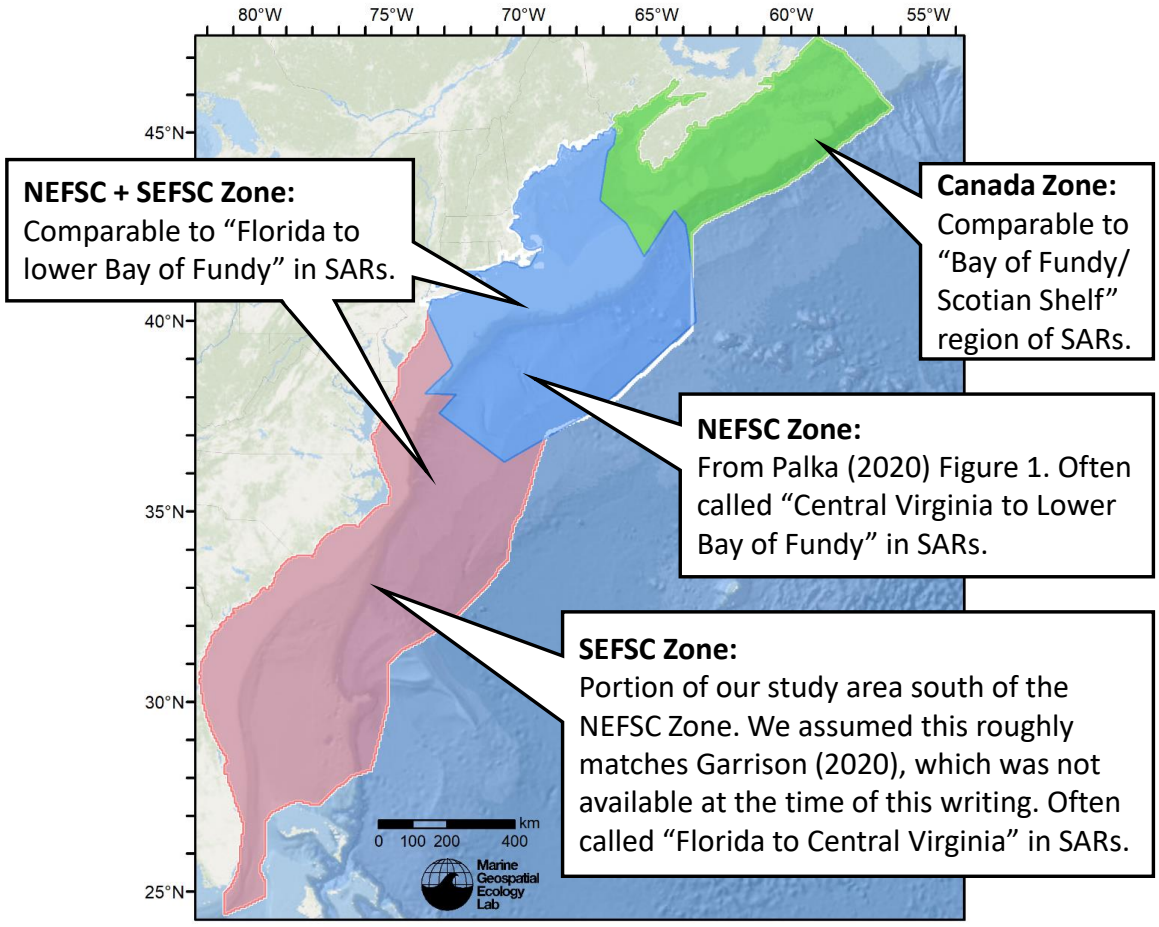

Figure 34: Zones for which we extracted abundance estimates from the density model for comparison to estimates from the NOAA Stock Assessment Report.

5.2.2 Previous Density Model

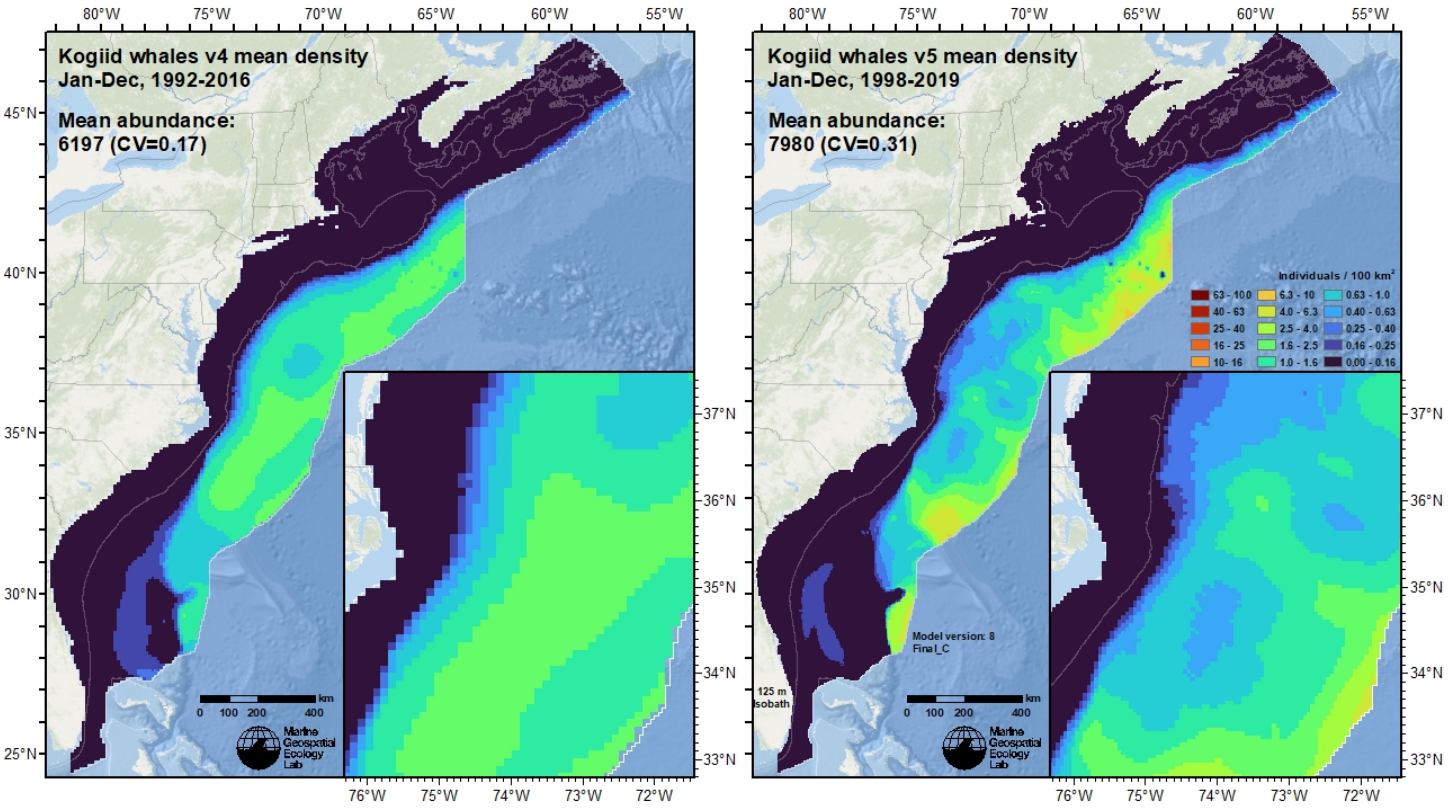

Figure 35: Comparison of the mean density predictions from the previous model (left) released by Roberts et al. (2017) to those from this model (right).

6 Discussion

The year-round mean abundance was 7,980 animals with highest abundance predicted in deep offshore ranges as well as near the slope north of Cape Hatteras, on the Blake Escarpment and south of Blake Spur. These predictions are largely in agreement with the findings of recent acoustic studies (Hodge et al. 2018; Cohen et al. 2022; Kowarski et al. 2022). Monthly predictions showed very little seasonal variation despite this being a contemporaneous model (Figure 32). The lowest predicted abundance was in October with 6,947 animals predicted and the highest abundance was in June with 9,268 animals predicted. This lent additional support to our decision to provide year-round mean abundance for this species.

The extrapolation statistics show some extrapolation in univariate space. Depth showed a few cells of extrapolated values at the eastern mid-Atlantic edge of the study area (Figure 27). The distance to eddy covariate showed some univariate extrapolation in all months except December (Figure 28). In this case distances "inside" the eddy ring are negative values, and the extrapolation cells indicate very large eddies, with large cores that are far from the ring in the negative direction. This was unlikely to be a major issue, as large eddies needed to trigger the extrapolation were infrequent and as such, unlikely to have yielded a big effect in the final model. Sea surface salinity showed swaths of out of range cells in the southwestern and southeastern edges of the study area in and around Blake Plateau in winter months and a few isolated out of range cells on the southwestern edge in spring (Figure 30). This was likely due to areas of high SSS and was unlikely to have yielded effects in the final model given the decreasing functional relationship (Figure 21).

In comparison to the SAR (Hayes et al. 2020) the abundance reported for the NEFSC region summer estimate (4,548) was similar to this model, with our year-round mean abundance predicting only about 15% fewer animals (3,846). In the SEFSC region our model predicted 14% more animals (3,739) from the year-round mean compared to the SAR summer estimate (3,202). This results in an overall 2% lower total abundance in the year-round estimate (7,585) for this species in comparison to the summer SAR estimate (7,750). Differences may be because the SAR estimates are based on a single year of summer survey data, whereas our estimates, are extracted from the year-round estimate, and are influenced by additional surveys, seasons, and years.

In comparison to the Roberts et al. (2017) model (6,197), mean abundance was 22% higher (1,783 animals) in the new model (7,980). However, it is important to note that the old model was climatological whereas this was a contemporaneous

model and as such, the higher predictions in winter and summer months in this model resulted in higher mean year-round abundance. The overall pattern in abundance and distribution was very similar between the two models.

References

Barco SG, Burt L, DePerte A, Digiovanni R Jr. (2015) Marine Mammal and Sea Turtle Sightings in the Vicinity of the Maryland Wind Energy Area July 2013-June 2015, VAQF Scientific Report #2015-06. Virginia Aquarium & Marine Science Center Foundation, Virginia Beach, VA

Becker JJ, Sandwell DT, Smith WHF, Braud J, Binder B, Depner J, Fabre D, Factor J, Ingalls S, Kim S-H, Ladner R, Marks K, Nelson S, Pharaoh A, Trimmer R, Von Rosenberg J, Wallace G, Weatherall P (2009) Global Bathymetry and Elevation Data at 30 Arc Seconds Resolution: SRTM30_PLUS. Marine Geodesy 32:355–371. doi: 10.1080/01490410903297766

Bloodworth BE, Odell DK (2008) Kogia breviceps (Cetacea: Kogiidae). Mammalian Species 819:1–12.

Buckland ST, Anderson DR, Burnham KP, Laake JL, Borchers DL, Thomas L (2001) Introduction to Distance Sampling: Estimating Abundance of Biological Populations. Oxford University Press, Oxford, UK

Burt ML, Borchers DL, Jenkins KJ, Marques TA (2014) Using mark-recapture distance sampling methods on line transect surveys. Methods in Ecology and Evolution 5:1180–1191. doi: 10.1111/2041-210X.12294

Chassignet E, Hurlburt H, Metzger EJ, Smedstad O, Cummings J, Halliwell G, Bleck R, Baraille R, Wallcraft A, Lozano C, Tolman H, Srinivasan A, Hankin S, Cornillon P, Weisberg R, Barth A, He R, Werner F, Wilkin J (2009) US GODAE: Global Ocean Prediction with the HYbrid Coordinate Ocean Model (HYCOM). Oceanog 22:64–75. doi: 10.5670/oceanog.2009.39

Chelton DB, Schlax MG, Samelson RM (2011) Global observations of nonlinear mesoscale eddies. Progress in Oceanography 91:167–216. doi: 10.1016/j.pocean.2011.01.002

Cohen RE, Frasier KE, Baumann-Pickering S, Wiggins SM, Rafter MA, Baggett LM, Hildebrand JA (2022) Identification of western North Atlantic odontocete echolocation click types using machine learning and spatiotemporal correlates. PLoS ONE 17:e0264988. doi: 10.1371/journal.pone.0264988

Cole T, Gerrior P, Merrick RL (2007) Methodologies of the NOAA National Marine Fisheries Service Aerial Survey Program for Right Whales (Eubalaena glacialis) in the Northeast U.S., 1998-2006. U.S. Department of Commerce, Woods Hole, MA

Cotter MP (2019) Aerial Surveys for Protected Marine Species in the Norfolk Canyon Region: 2018–2019 Final Report. HDR, Inc., Virginia Beach, VA

Foley HJ, Paxton CGM, McAlarney RJ, Pabst DA, Read AJ (2019) Occurrence, Distribution, and Density of Protected Species in the Jacksonville, Florida, Atlantic Fleet Training and Testing (AFTT) Study Area. Duke University Marine Lab, Beaufort, NC

Garrison LP (2020) Abundance of cetaceans along the southeast U.S. East coast from a summer 2016 vessel survey. PRD Contribution # PRD-2020-04. NOAA National Marine Fisheries Service, Southeast Fisheries Science Center, Miami, FL

Garrison LP, Martinez A, Maze-Foley K (2010) Habitat and abundance of cetaceans in Atlantic Ocean continental slope waters off the eastern USA. Journal of Cetacean Research and Management 11:267–277.

Harris PT, Macmillan-Lawler M, Rupp J, Baker EK (2014) Geomorphology of the oceans. Marine Geology 352:4–24. doi: 10.1016/j.margeo.2014.01.011

Hayes SA, Josephson E, Maze-Foley K, Rosel PE, Byrd B, Chavez-Rosales S, Cole TV, Garrison LP, Hatch J, Henry A, Horstman SC, Litz J, Lyssikatos MC, Mullin KD, Orphanides C, Pace RM, Palka DL, Powell J, Wenzel FW (2020) US Atlantic and Gulf of Mexico Marine Mammal Stock Assessments - 2019. NOAA National Marine Fisheries Service, Northeast Fisheries Science Center, Woods Hole, MA

Hayes SA, Josephson E, Maze-Foley K, Rosel PE, Wallace J, Brossard A, Chavez-Rosales S, Cole TVN, Garrison LP, Hatch J, Henry A, Horstman SC, Litz J, Lyssikatos MC, Mullin KD, Murray K, Orphanides C, Ortega-Ortiz J, Pace RM, Palka DL, Powell J, Rappucci G, Soldevilla M, Wenzel FW (2022) US Atlantic and Gulf of Mexico Marine Mammal Stock Assessments 2021. NOAA National Marine Fisheries Service, Northeast Fisheries Science Center, Woods Hole, MA

Hodge LEW, Baumann-Pickering S, Hildebrand JA, Bell JT, Cummings EW, Foley HJ, McAlarney RJ, McLellan WA, Pabst DA, Swaim ZT, Waples DM, Read AJ (2018) Heard but not seen: Occurrence of *Kogia* spp. Along the western North Atlantic shelf break: NOTES. Mar Mam Sci 34:1141–1153. doi: 10.1111/mms.12498

Jefferson TA, Schiro AJ (1997) Distribution of cetaceans in the offshore Gulf of Mexico. Mammal Review 27:27–50. doi: 10.1111/j.1365-2907.1997.tb00371.x

Kowarski KA, Martin SB, Maxner EE, Lawrence CB, Delarue JJ-Y, Miksis-Olds JL (2022) Cetacean acoustic occurrence on the US Atlantic Outer Continental Shelf from 2017 to 2020. Marine Mammal Science mms.12962. doi: 10.1111/mms.12962

Laake JL, Calambokidis J, Osmek SD, Rugh DJ (1997) Probability of Detecting Harbor Porpoise From Aerial Surveys: Estimating g(0). Journal of Wildlife Management 61:63–75. doi: 10.2307/3802415

Lehodey P, Senina I, Murtugudde R (2008) A spatial ecosystem and populations dynamics model (SEAPODYM)–Modeling of tuna and tuna-like populations. Progress in Oceanography 78:304–318. doi: 10.1016/j.pocean.2008.06.004

Lehodey P, Conchon A, Senina I, Domokos R, Calmettes B, Jouanno J, Hernandez O, Kloser R (2015) Optimization of a micronekton model with acoustic data. ICES Journal of Marine Science 72:1399–1412. doi: 10.1093/icesjms/fsu233

Leiter S, Stone K, Thompson J, Accardo C, Wikgren B, Zani M, Cole T, Kenney R, Mayo C, Kraus S (2017) North Atlantic right whale Eubalaena glacialis occurrence in offshore wind energy areas near Massachusetts and Rhode Island, USA. Endang Species Res 34:45–59. doi: 10.3354/esr00827

Mallette SD, Lockhart GG, McAlarney RJ, Cummings EW, McLellan WA, Pabst DA, Barco SG (2014) Documenting Whale Migration off Virginia's Coast for Use in Marine Spatial Planning: Aerial and Vessel Surveys in the Proximity of the Virginia Wind Energy Area (VA WEA), VAQF Scientific Report 2014-08. Virginia Aquarium & Marine Science Center Foundation, Virginia Beach, VA

Mallette SD, Lockhart GG, McAlarney RJ, Cummings EW, McLellan WA, Pabst DA, Barco SG (2015) Documenting Whale Migration off Virginia's Coast for Use in Marine Spatial Planning: Aerial Surveys in the Proximity of the Virginia Wind Energy Area (VA WEA) Survey/Reporting Period: May 2014 - December 2014, VAQF Scientific Report 2015-02. Virginia Aquarium & Marine Science Center Foundation, Virginia Beach, VA

Mallette SD, McAlarney RJ, Lockhart GG, Cummings EW, Pabst DA, McLellan WA, Barco SG (2017) Aerial Survey Baseline Monitoring in the Continental Shelf Region of the VACAPES OPAREA: 2016 Annual Progress Report. Virginia Aquarium & Marine Science Center Foundation, Virginia Beach, VA

Marsh H, Sinclair DF (1989) Correcting for Visibility Bias in Strip Transect Aerial Surveys of Aquatic Fauna. The Journal of Wildlife Management 53:1017. doi: 10.2307/3809604

McAlarney R, Cummings E, McLellan W, Pabst A (2018) Aerial Surveys for Protected Marine Species in the Norfolk Canyon Region: 2017 Annual Progress Report. University of North Carolina Wilmington, Wilmington, NC

McLellan WA, McAlarney RJ, Cummings EW, Read AJ, Paxton CGM, Bell JT, Pabst DA (2018) Distribution and abundance of beaked whales (Family Ziphiidae) Off Cape Hatteras, North Carolina, U.S.A. Marine Mammal Science. doi: 10.1111/mms.12500

Merkens K, Mann D, Janik VM, Claridge D, Hill M, Oleson E (2018) Clicks of dwarf sperm whales (*Kogia Sima*). Mar Mam Sci 34:963–978. doi: 10.1111/mms.12488

Mesgaran MB, Cousens RD, Webber BL (2014) Here be dragons: A tool for quantifying novelty due to covariate range and correlation change when projecting species distribution models. Diversity Distrib 20:1147–1159. doi: 10.1111/ddi.12209

Miller DL, Becker EA, Forney KA, Roberts JJ, Cañadas A, Schick RS (2022) Estimating uncertainty in density surface models. PeerJ 10:e13950. doi: 10.7717/peerj.13950

Mullin KD, Fulling GL (2003) Abundance of cetaceans in the southern U.S. North Atlantic Ocean during summer 1998. Fishery Bulletin 101:603–613.

O'Brien O, Pendleton DE, Ganley LC, McKenna KR, Kenney RD, Quintana-Rizzo E, Mayo CA, Kraus SD, Redfern JV (2022) Repatriation of a historical North Atlantic right whale habitat during an era of rapid climate change. Sci Rep 12:12407. doi: 10.1038/s41598-022-16200-8

Palka D (2020) Cetacean Abundance in the US Northwestern Atlantic Ocean Summer 2016. Northeast Fish Sci Cent Ref Doc. 20-05. NOAA National Marine Fisheries Service, Northeast Fisheries Science Center, Woods Hole, MA

Palka D, Aichinger Dias L, Broughton E, Chavez-Rosales S, Cholewiak D, Davis G, DeAngelis A, Garrison L, Haas H, Hatch J, Hyde K, Jech M, Josephson E, Mueller-Brennan L, Orphanides C, Pegg N, Sasso C, Sigourney D, Soldevilla M, Walsh H (2021) Atlantic Marine Assessment Program for Protected Species: FY15 – FY19 (OCS Study BOEM 2021-051). U.S. Deptartment of the Interior, Bureau of Ocean Energy Management, Washington, DC

Palka DL (2006) Summer abundance estimates of cetaceans in US North Atlantic navy operating areas (NEFSC Reference Document 06-03). U.S. Department of Commerce, Northeast Fisheries Science Center, Woods Hole, MA

Palka DL, Chavez-Rosales S, Josephson E, Cholewiak D, Haas HL, Garrison L, Jones M, Sigourney D, Waring G, Jech M, Broughton E, Soldevilla M, Davis G, DeAngelis A, Sasso CR, Winton MV, Smolowitz RJ, Fay G, LaBrecque E, Leiness JB, Dettloff K, Warden M, Murray K, Orphanides C (2017) Atlantic Marine Assessment Program for Protected Species: 2010-2014 (OCS Study BOEM 2017-071). U.S. Deptartment of the Interior, Bureau of Ocean Energy Management, Washington, DC

Quintana-Rizzo E, Leiter S, Cole T, Hagbloom M, Knowlton A, Nagelkirk P, O'Brien O, Khan C, Henry A, Duley P, Crowe L, Mayo C, Kraus S (2021) Residency, demographics, and movement patterns of North Atlantic right whales Eubalaena glacialis in an offshore wind energy development area in southern New England, USA. Endang Species Res 45:251–268. doi: 10.3354/esr01137

Read AJ, Barco S, Bell J, Borchers DL, Burt ML, Cummings EW, Dunn J, Fougeres EM, Hazen L, Hodge LEW, Laura A-M, McAlarney RJ, Peter N, Pabst DA, Paxton CGM, Schneider SZ, Urian KW, Waples DM, McLellan WA (2014) Occurrence, distribution and abundance of cetaceans in Onslow Bay, North Carolina, USA. Journal of Cetacean Research and Management 14:23–35.

Redfern JV, Kryc KA, Weiss L, Hodge BC, O'Brien O, Kraus SD, Quintana-Rizzo E, Auster PJ (2021) Opening a Marine Monument to Commercial Fishing Compromises Species Protections. Front Mar Sci 8:645314. doi: 10.3389/fmars.2021.645314

Roberts JJ, Best BD, Dunn DC, Treml EA, Halpin PN (2010) Marine Geospatial Ecology Tools: An integrated framework for ecological geoprocessing with ArcGIS, Python, R, MATLAB, and C++. Environmental Modelling & Software 25:1197–1207. doi: 10.1016/j.envsoft.2010.03.029

Roberts JJ, Best BD, Mannocci L, Fujioka E, Halpin PN, Palka DL, Garrison LP, Mullin KD, Cole TVN, Khan CB, McLellan WA, Pabst DA, Lockhart GG (2016) Habitat-based cetacean density models for the U.S. Atlantic and Gulf of Mexico. Scientific Reports 6:22615. doi: 10.1038/srep22615

Roberts JJ, Mannocci L, Halpin PN (2017) Final Project Report: Marine Species Density Data Gap Assessments and Update for the AFTT Study Area, 2016-2017 (Opt. Year 1), Document Version 1.4. Duke University Marine Geospatial Ecology Lab, Durham, NC

Roberts JJ, Yack TM, Halpin PN (2023) Marine mammal density models for the U.S. Navy Atlantic Fleet Training and Testing (AFTT) study area for the Phase IV Navy Marine Species Density Database (NMSDD), Document Version 1.3. Duke University Marine Geospatial Ecology Lab, Durham, NC

Robertson FC, Koski WR, Brandon JR, Thomas TA, Trites AW (2015) Correction factors account for the availability of bowhead whales exposed to seismic operations in the Beaufort Sea. Journal of Cetacean Research and Management 15:35–44.

Schlax MG, Chelton DB (2016) The "Growing Method" of Eddy Identification and Tracking in Two and Three Dimensions. College of Earth, Ocean and Atmospheric Sciences, Oregon State University, Corvallis, OR

Staudinger MD, McAlarney RJ, McLellan WA, Ann Pabst D (2014) Foraging ecology and niche overlap in pygmy (*Kogia Breviceps*) and dwarf (*Kogia Sima*) sperm whales from waters of the U.S. Mid-Atlantic coast. Marine Mammal Science 30:626–655. doi: 10.1111/mms.12064

Stone KM, Leiter SM, Kenney RD, Wikgren BC, Thompson JL, Taylor JKD, Kraus SD (2017) Distribution and abundance of cetaceans in a wind energy development area offshore of Massachusetts and Rhode Island. J Coast Conserv 21:527–543. doi: 10.1007/s11852-017-0526-4

Torres LG, Mclellan WA, Meagher E, Pabst DA (2005) Seasonal distribution and relative abundance of bottlenose dolphins, Tursiops truncatus, along the US mid-Atlantic coast. Journal of Cetacean Research and Management 7:153.

Waring GT (2013) Appendix IV: Summary of surveys and abundance estimates (from NOAA 2012 SAR).

Willis PM, Baird RW (1998) Status of the dwarf sperm whale, Kogia simus, with special reference to Canada. Canadian Field-Naturalist 112:114–125.

Zoidis AM, Lomac-MacNair KS, Ireland DS, Rickard ME, McKown KA, Schlesinger MD (2021) Distribution and density of six large whale species in the New York Bight from monthly aerial surveys 2017 to 2020. Continental Shelf Research 230:104572. doi: 10.1016/j.csr.2021.104572